

## ZFP281 ORCHESTRATES INTERCONVERSION OF PLURIPOTENT STATES BY ENGAGING EHMT1 AND ZIC2

Daniela Mayer<sup>1,2</sup>, Michael B. Stadler<sup>1,3</sup>, Melanie Rittirsch<sup>1</sup>, Daniel Hess<sup>1</sup>, Ilya Lukonin<sup>1,2</sup>, Maria Winzi<sup>4</sup>, Austin Smith<sup>5</sup>, Frank Buchholz<sup>4</sup>, Joerg Betschinger<sup>1,\*</sup>

<sup>1</sup>Friedrich Miescher Institute for Biomedical Research, 4058 Basel, Switzerland

<sup>2</sup>Faculty of Sciences, University of Basel, 4003 Basel, Switzerland

<sup>3</sup>Swiss Institute of Bioinformatics, 4058 Basel, Switzerland

<sup>4</sup>Medical Systems Biology, UCC, Medical Faculty Carl Gustav Carus, TU Dresden, 01307 Dresden, Germany

<sup>5</sup>Wellcome-MRC Cambridge Stem Cell Institute and Department of Biochemistry, University of Cambridge, Cambridge CB2 1QR, United Kingdom

1 \*lead contact: joerg.betschinger@fmi.ch

1 **ABSTRACT**

2 Developmental cell fate specification is a unidirectional process that can be reverted in response to  
3 injury or experimental reprogramming. Whether differentiation and de-differentiation trajectories  
4 intersect mechanistically is unclear. Here, we performed comparative screening in lineage-related  
5 mouse naïve embryonic stem cells (ESCs) and primed epiblast stem cells (EpiSCs), and identified the  
6 constitutively expressed zinc finger transcription factor (TF) Zfp281 as a bi-directional regulator of cell  
7 state interconversion. We showed that subtle chromatin binding changes in differentiated cells translate  
8 into activation of the histone H3 lysine 9 (H3K9) methyltransferase Ehmt1 and stabilization of the zinc  
9 finger TF Zic2 at enhancers and promoters. Genetic gain- and loss-of-function experiments confirmed  
10 a critical role of Ehmt1 and Zic2 downstream of Zfp281 both in driving exit from the ESC state, and in  
11 restricting reprogramming of EpiSCs. Our study reveals that cell type-invariant chromatin association  
12 of Zfp281 provides an interaction platform for remodeling the cis-regulatory network underlying cellular  
13 plasticity.

14

15 **INTRODUCTION**

16 Mammalian development is a hierarchical process that coordinates organismal growth with increasing  
17 cellular differentiation. The lineage progression of the few pluripotent cells in the blastocyst towards the  
18 many specialized cell types in the mature embryo is by and large unidirectional. However, fully  
19 differentiated cells can be de-differentiated into induced pluripotent stem cells (iPSCs) by ectopic  
20 expression of the transcription factors (TFs) Oct4, Sox2, Klf4 and c-Myc (Takahashi & Yamanaka,  
21 2006). Reprogramming of somatic cells into iPSCs requires erasure of the entire developmental history  
22 of a somatic cell, but whether this depends on the reversal of developmental hierarchies is unclear  
23 (Ladewig *et al*, 2013; Takahashi & Yamanaka, 2015).

24 Transcriptional and epigenomic profiling of the reprogramming process has revealed an ordered series  
25 of events that include the transient and sequential activation of late and early developmental genes  
26 (Cacchiarelli *et al*, 2015; Amlani *et al*, 2018; Takahashi *et al*, 2014). Although the specific trajectory is  
27 dictated by the identity of the starting somatic cell type (Nefzger *et al*, 2017; Jackson *et al*, 2016) and  
28 the experimental regime (Chantzoura *et al*, 2015; Stuart *et al*, 2019), iPSC formation may involve the  
29 reversion of natural developmental mechanisms (Takahashi & Yamanaka, 2015). Consistent with this  
30 possibility, a mesenchymal-to-epithelial transition is necessary for iPSC formation (Samavarchi-Tehrani  
31 *et al*, 2010; Li *et al*, 2010), while the converse epithelial-to-mesenchymal transition is crucial for  
32 embryogenesis, e.g. during gastrulation and neural crest formation (Acloque *et al*, 2009). Although it is  
33 debated if these observations reflect a shared developmental intermediate (Raab *et al*, 2017), they  
34 suggest that de-differentiation and differentiation employ common mechanisms in opposite directions.  
35 Here, we systematically and functionally examine this concept using naïve pluripotent embryonic stem  
36 cells (ESCs) and primed pluripotent epiblast stem cells (EpiSCs) (Smith, 2017).

37 ESCs and EpiSCs are developmentally related derivatives of mouse embryonic day (E) 3.75-4.5  
38 blastocysts (Boroviak *et al*, 2014) and E5.5-8.0 embryos (Tesar *et al*, 2007; Brons *et al*, 2007; Osorno

1 *et al*, 2012), respectively. ESCs cultured in the presence of two inhibitors (2i) resemble naïve pluripotent  
2 cells of the pre-implantation epiblast (Boroviak *et al*, 2014), while primed pluripotent EpiSCs cultured in  
3 the presence of FGF2 and Activin A (FA) resemble cells of the late gastrula (Osorno *et al*, 2012;  
4 Tsakiridis *et al*, 2014; Kojima *et al*, 2014). Upon *in vitro* differentiation, ESCs progress through a  
5 transient post-implantation epiblast-like (EpiLC) cell state that is amenable to EpiSC derivation (Zhang  
6 *et al*, 2010; Hayashi *et al*, 2011). Conversely, activation of just one TF, such as Stat3, Klf4, or Esrrb, is  
7 sufficient to reprogram EpiSCs into naïve pluripotent EpiSC-derived iPSCs (Epi-iPSCs) in the presence  
8 of 2i (Yang *et al*, 2010; Guo *et al*, 2009; Festuccia *et al*, 2012). The interconvertibility of ESCs and  
9 EpiSCs thus provides an experimental system to explore if de-differentiation includes the reversion of  
10 differentiation mechanisms.

11 Using a large-scale loss-of-function reprogramming screen in sensitized EpiSCs we identify the zinc  
12 finger TF Zfp281 as a prominent bidirectional ESC-EpiSC transition regulator. We show that Zfp281  
13 exhibits stable chromatin association and drives ESC progression through differentiation-specific  
14 interaction with Ehmt1 and Zic2. Genomic analysis revealed activation of Ehmt1 and enrichment of Zic2  
15 at Zfp281-bound cis-regulatory elements (CREs) that are associated with developmental transcription  
16 in EpiLCs and EpiSCs. Zfp281, therefore, establishes and stabilizes cell fate commitment to safeguard  
17 the unidirectionality of pluripotent state transitions.

18

## 19 **RESULTS**

### 20 **Zfp281 is a bidirectional ESC-EpiSC transition regulator**

21 We hypothesized that mechanisms common to differentiation and de-differentiation may be encoded in  
22 genes that both promote exit from the naïve ESC state and impair reprogramming of EpiSCs. ESC  
23 differentiation drivers have been determined in several genetic loss of function screens (Betschinger *et al*,  
24 2013; Li *et al*, 2018; Leeb *et al*, 2014; Guo *et al*, 2011; Westerman *et al*, 2011), but it is unknown if  
25 those also inhibit reprogramming of EpiSCs into naïve pluripotency. We therefore set out to  
26 systematically identify reprogramming roadblocks using a large-scale endoribonuclease-prepared small  
27 interfering RNA (esiRNA) loss-of-function screen (Ding *et al*, 2009). We made use of O4GIP<sub>GY118F</sub>  
28 EpiSCs expressing green fluorescent protein (GFP) and Puromycin N-acetyl-transferase under the  
29 regulatory sequences of the *Oct4* gene (Guo *et al*, 2009), and a Stat3 activating receptor (GY118F)  
30 responsive to granulocyte colony stimulating factor (Gcsf) driven by a constitutive promoter (Yang *et al*,  
31 2010). Upon exposure to Gcsf and 2i for 4 days (d), O4GIP<sub>GY118F</sub> EpiSCs gave rise to self-renewing  
32 Epi-iPSCs at an efficiency of roughly 0.1% (Figure **EV1A**), thus providing a sensitized setup to identify  
33 reprogramming inhibitors. O4GIP<sub>GY118F</sub> EpiSCs were transfected with esiRNAs targeting 9540  
34 transcripts and control esiRNAs targeting Luciferase (Luc) and the GY118F downstream effector Stat3  
35 in 384 well plates (Figure **1A**). The next day, reprogramming was induced by changing to 2i and Gcsf.  
36 After 4d, we selected Epi-iPSCs in the presence of Puromycin, and quantified viability with a fluorescent  
37 assay after 3-4d. The screen was performed in duplicate and Z scores were calculated per plate (Table  
38 **EV1**). Positive (Stat3 esiRNA), but not negative (non-targeting Luc esiRNA and no esiRNA) controls  
39 induced negative Z scores (Figure **EV1B**). Screen hits with average Z scores < -2 included ribosome

1 and proteasome subunits, Stat3 and Oct4 (Figure **1B**), and were strongly enriched for functions  
2 associated with RNA maturation and translation using gene ontology (GO) analysis (Figure **EV1C**).  
3 These therefore contain genes required for reprogramming and/or cell survival. Screen hits with positive  
4 Z scores, conversely, are expected to inhibit reprogramming and/or proliferation. Among the 146 hits  
5 with an average Z score > 2, the zinc finger TF *Zfp281* and the E3 ubiquitin ligase *Fbxw7* scored highest.  
6 *Zfp281* and *Fbxw7* have previously been shown to restrict iPSC generation from somatic cells (Fidalgo  
7 *et al*, 2012; Buckley *et al*, 2012; Okita *et al*, 2012; Fidalgo *et al*, 2016), thus suggesting successful  
8 identification of reprogramming roadblocks.

9 To determine if any of the 146 genes also drive ESC differentiation, we compared our screen hits with  
10 those from two previous large-scale ESC differentiation loss-of-function studies (Betschinger *et al*,  
11 2013; Li *et al*, 2018) (Figure **1C**). *Zfp281* and the cytochrome c oxidase subunits *Cox5a* and *Cox6c*  
12 scored strongest in all screens. For validation, we depleted each of them by siRNA transfection in  
13 independent GY118F-expressing Oct4 reporter 796.4 EpiSCs (Yang *et al*, 2010) and also included  
14 siRNAs targeting *Fbxw7* and *Tcf7l1* as controls (Figure **1B, C**). Knockdown of *Fbxw7* and *Zfp281*, but  
15 not of *Cox5a*, *Cox6c* or *Tcf7l1* increased reprogramming (Figure **1D, EV1D**). Therefore, *Cox5a* and  
16 *Cox6c* are false-positive or cell line-dependent screen hits, and we focused our further efforts on  
17 *Zfp281*. Consistent with previous findings (Fidalgo *et al*, 2016), Epi-iPSCs derived by *Zfp281* depletion  
18 expressed the naïve TFs *Esrrb*, *Klf4*, *Nr0b1* and *Tbx3*, and reduced levels of the primed markers *Oct6*,  
19 *Fgf5*, *Sox3* and *Dnmt3b* (Figure **EV1E**), suggesting successful reversion to the pluripotent ground state.

20 To quantify the dynamics of this process, we used self-renewal in 2i as a proxy for acquisition of Epi-  
21 iPSC identity. Compared to controls, *Zfp281* depletion dramatically increased the colony forming  
22 capacity of single cells after 2d and 4d of *Gcsf* addition (Figure **1E**), indicating accelerated and more  
23 efficient reprogramming of EpiSCs. *Gcsf* supplementation was essential and co-depletion of *Stat3*  
24 abolished Epi-iPSC formation from O4GIP<sub>GY118F</sub> EpiSCs in the presence of *Gcsf* (Figure **EV1F**).  
25 Similarly, Leukemia inhibitory factor (*Lif*), which activates *Stat3* in EpiSCs (Yang *et al*, 2010), was  
26 required for reprogramming of *Zfp281*-depleted OEC2 EpiSCs (Figure **1F**). To test if *Zfp281* acts only  
27 in the context of active *Stat3*, we used conditional expression of *Esrrb* or *Klf4* in O4GIP EpiSCs through  
28 addition of Doxycycline (*Dox*) to induce reprogramming. In the absence of extrinsic *Lif* we observed an  
29 increase in *Dox*-induced Epi-iPSC colonies upon knockdown of *Zfp281* (Figure **1G**), suggesting that  
30 *Zfp281* functions independent of the specific reprogramming regime. Taken together these findings  
31 demonstrate that the vast majority of cell state transition regulators act unidirectionally. *Zfp281*, in  
32 contrast, acts bidirectionally as it drives ESC differentiation and inhibits reprogramming of EpiSCs.  
33 Notably, this is inverse to the activity of reprogramming TFs, e.g. *Klf4* and *Esrrb*, that induce and  
34 consolidate the naïve ESC state (Yamane *et al*, 2018; Festuccia *et al*, 2012; Guo *et al*, 2009; Martello  
35 *et al*, 2012; Niwa *et al*, 2009).

### 36 ***Zfp281* promotes exit from naïve pluripotency independent of *Tet1* and *Tet2***

37 To characterize the function of *Zfp281* in ESC differentiation, we inactivated the gene in naïve RGd2  
38 ESCs that contain a destabilized GFP protein downstream of the *Rex1* (*Zfp42*) promoter (Figure **EV2A**,  
39 **B**) which allows near real-time tracking of cell state transition (Kalkan *et al*, 2017): GFP is

1 homogeneously expressed in 2i and up to 16 hours (h) after 2i withdrawal (GFP<sub>high</sub>) (Kalkan *et al*, 2017)  
2 before becoming progressively downregulated (GFP<sub>low</sub>) as ESCs exit from self-renewal (Figure **EV2C**).  
3 In 2i, reporter expression in two independent *Zfp281* knockout (KO) clones was similar to the parental  
4 wildtype cell line (*WT*) and an untargeted wildtype sibling clone (*Zfp281* WT) (Figure **EV2D**). In contrast,  
5 32h and 72h after 2i withdrawal, 30% and less than 1% of *WT* cells were GFP<sub>high</sub>, while 75% and 10%  
6 of *Zfp281* KO cells maintained high GFP expression, respectively. Consistent with impaired exit from  
7 the ESC state, 10% of *Zfp281* KO cells formed colonies in 2i after 72h of differentiation (Figure **2A**).  
8 This phenotype was reverted by transgenic *Zfp281* expression (Figure **2B**). Resistance to exit self-  
9 renewal was also observed in KO cells generated in a different ESC line (Figure **EV2A, B, E**), and in  
10 EpiLC (Hayashi *et al*, 2011) and embryoid body (EB) differentiation regimes (Figure **2A, EV2D**). *Zfp281*  
11 mutant cells maintained *Rex1* reporter expression and self-renewal even after lengthy periods in the  
12 absence of 2i (Figure **2A, EV2D**), demonstrating that differentiation resistance is persistent.

13 Differentiating *Zfp281* KO cells expressed varied levels of the *Rex1* reporter (Figure **EV2D**) and formed  
14 colonies in 2i less efficiently than naïve pluripotent ESCs. E.g. 32h after 2i withdrawal, mutant cells  
15 displayed only 40% of the self-renewal capacity of ESCs (Figure **EV1F**). To test if this reduction is linked  
16 to population heterogeneity, we purified GFP<sub>high</sub> and GFP<sub>low</sub> cells at 32h using fluorescence-activated  
17 cell sorting. As expected (Kalkan *et al*, 2017), sorted *WT* GFP<sub>low</sub> cells were largely committed to  
18 differentiation and unable to generate clones in 2i (Figure **2C**). In contrast, *Zfp281* KO GFP<sub>low</sub> cells  
19 formed colonies almost as efficiently as GFP<sub>high</sub> cells. *Rex1* downregulation and exit from the ESC state  
20 is, thus, disconnected in *Zfp281* mutants. However, the efficiency with which GFP<sub>high</sub> cells formed  
21 colonies after 32h of 2i withdrawal was lower than of GFP<sub>high</sub> cells after 24h (Kalkan *et al*, 2017) and of  
22 ESCs (Figure **2C**). This was irrespective of genotype, suggesting a gradual decline of self-renewal  
23 during differentiation both in *Zfp281* mutant and *WT* GFP<sub>high</sub> cells. The reduced clonogenicity of *Zfp281*  
24 KO populations compared to ESCs may therefore be consequential to impaired progression of an  
25 advanced cell state with limited self-renewal capacity and independent of population heterogeneity. In  
26 fact, GFP<sub>low</sub> cells in long-term differentiated *Zfp281* mutants re-established GFP<sub>high</sub> expression within a  
27 few days (Figure **EV2G**), revealing reversibility of the GFP<sub>low</sub> state in the absence of *Zfp281*. To test  
28 sufficiency, we generated naïve RGd2 cells conditionally overexpressing *Zfp281* under Dox regulation  
29 (Figure **EV2H**). Dox-treatment in the presence of 2i induced silencing of the *Rex1* reporter and loss of  
30 self-renewal in a subset of cells (Figure **2D, EV2I**). *Zfp281* is therefore required and sufficient for exit  
31 from naïve pluripotency.

32 A previous study showed that differentiation of Serum/Lif-cultured ESCs is accompanied by up-  
33 regulation of *Zfp281*, which in turn destabilizes metastable pluripotency by binding to the methylcytosine  
34 hydroxylase Tet1 and transcriptionally suppressing Tet2 (Fidalgo *et al*, 2016). If the same mechanisms  
35 were to regulate exit from naïve pluripotency downstream of *Zfp281*, loss of *Tet1* should induce the  
36 same phenotype as loss of *Zfp281*, and loss of *Tet2* the opposite. We therefore generated *Tet1*, *Tet2*  
37 and *Zfp281/Tet2* KO alleles in naïve RGd2 ESCs (Figure **EV2J, K**). Strikingly, the extinction of the *Rex1*  
38 reporter and self-renewal was similar in differentiating *WT* cells and *Tet1* and *Tet2* mutants, while  
39 absence of *Tet2* in *Zfp281/Tet2* KO cells did not revert resistance to differentiation caused by absence  
40 of *Zfp281* alone (Figure **2E, EV2L**). We furthermore noted only modest changes in *Zfp281* mRNA or

1 protein during ESC differentiation, and across existing RNA sequencing (RNA-seq) datasets of EpiLC  
2 and EpiSC differentiation (Buecker *et al*, 2014; Factor *et al*, 2014; Bao *et al*, 2018) and epiblast  
3 development (Boroviak *et al*, 2015) (Figure **2F**, **EV2M**). Zfp281 has also been reported to repress *Nanog*  
4 transcription through interacting with the NuRD complex in Serum/Lif-cultured ESCs (Fidalgo *et al*,  
5 2012). However, *Nanog* mRNA was unchanged in naïve *Zfp281* KO ESCs or EpiSCs depleted of  
6 Zfp281 by siRNA transfection (Figure **EV2N**, **O**). Furthermore, knockdown of *Nanog* did not restore  
7 differentiation in ESCs depleted of Zfp281 while it partially did so, as expected (Pereira *et al*, 2006), in  
8 ESCs depleted of Tcf711 (Figure **EV2P**). Taken together these results suggest that Zfp281 is expressed  
9 fairly constantly during exit from naïve pluripotency and drives differentiation independent of Tet1, Tet2  
10 and *Nanog*.

### 11 **Zfp281 acts independent of cell state-exclusive chromatin association**

12 To identify the transcriptional defects causing differentiation resistance, we performed RNA-seq of *WT*  
13 and *Zfp281* KO cells in 2i, and 16h and 32h after 2i withdrawal (*WT*<sub>2i,16h,32h</sub> and *Zfp281*<sub>2i,16h,32h</sub>) (Table  
14 **EV2**). The expression of several naïve and primed pluripotency markers was perturbed in *Zfp281*<sub>16h</sub>  
15 and *Zfp281*<sub>32h</sub> cells (Figure **EV3A**), confirming impaired silencing of naïve identity in *Zfp281* mutants.  
16 k-means clustering of mRNAs that significantly changed during *WT* differentiation or in *Zfp281* KO cells  
17 (2495 genes) identified six gene clusters (Figure **3A**, **B**): Clusters 1-4 (1898 genes) contain the majority  
18 of genes that were differentially transcribed in *WT*<sub>32h</sub> cells and of which a subset was already regulated  
19 in *WT*<sub>16h</sub> cells. Comparison with external EpiLC (Buecker *et al*, 2014) and EpiSC (Factor *et al*, 2014;  
20 Bao *et al*, 2018) expression datasets, which were not employed in the clustering analysis, revealed  
21 persistence of the bulk transcriptional changes established in *WT*<sub>32h</sub> cells, suggesting that clusters 1-4  
22 contribute to pluripotent cell state progression. Clusters 5 and 6 (597 genes), in contrast, contain genes  
23 that were mostly unchanged in *WT*<sub>32h</sub> cells, but transiently regulated in *WT*<sub>16h</sub> cells and differentially  
24 expressed in EpiSCs. Clusters 5 and 6 may therefore act in gastrulation stage epiblast development  
25 and/or EpiSCs.

26 Clusters 1 and 2 were largely unaffected in differentiating *Zfp281* KO cells, whereas the repression and  
27 induction, respectively, of cluster 3 and 4 genes was blunted in both *Zfp281*<sub>16h</sub> and *Zfp281*<sub>32h</sub> cells  
28 (Figure **3A**, **B**). Cell state-specific comparison revealed that this was predominantly due to deregulation  
29 during differentiation (Figure **3C**). Although we can't exclude that the transcriptional defects in *Zfp281*<sub>32h</sub>  
30 cells were influenced by cell state heterogeneity (Figure **EV2D**), perturbed expression of cluster 3 and  
31 4 genes in *Zfp281*<sub>16h</sub> cells, a timepoint at which downregulation of Rex1 reporter expression (Kalkan *et al*,  
32 2017) and exit from self-renewal (Figure **EV2C**, **F**) has not yet commenced, suggests a direct role  
33 of Zfp281 in regulating these genes. Zfp281 may therefore drive exit from naïve pluripotency through  
34 controlling gene clusters 3 and 4, which contain the naïve pluripotency TFs *Klf4*, *Klf5* and *NrOb1*, and  
35 the primed markers *Sox3* and *Dnmt3b*, respectively (Table **EV2**), and are enriched for generic  
36 developmental terms using GO analysis (Figure **EV3B**). Conversely, cluster 5 and 6 genes were  
37 similarly mis-expressed in *Zfp281*<sub>2i</sub>, *Zfp281*<sub>16h</sub> and *Zfp281*<sub>32h</sub> cells, notably with directionalities that are  
38 inverse to the changes observed in EpiSCs. GO analysis revealed significant enrichment of regulators  
39 of cell adhesion, which is critical for cell polarization (Ebnet *et al*, 2018) that initiates lumenogenesis

1 after exit from naïve pluripotency (Shahbazi *et al*, 2017). To test if Zfp281 controls polarization, we  
2 generated spheroids in Matrigel as described before (Shahbazi *et al*, 2017). WT ESCs formed polarized  
3 spheroids with expanded lumens that were encircled by apical F-actin, while *Zfp281* KO cells grew as  
4 unpolarized and disorganized cellular aggregates that were morphologically similar to ESCs (Figure  
5 **3D**). Although we cannot exclude that this is consequential to impaired exit from self-renewal, regulation  
6 of cluster 5 and 6 genes by Zfp281 may therefore contribute to cell polarization and cavity formation  
7 during ESC differentiation.

8 Oct4, similar to Zfp281, is expressed at equal levels in ESCs and EpiLCs, but occupies distinct CREs  
9 in the two cell states (Buecker *et al*, 2014). To determine if Zfp281 acts through cell state-specific  
10 chromatin association, we profiled its genome localization in *WT*<sub>2i</sub> and *WT*<sub>32h</sub> cells using chromatin  
11 immunoprecipitation coupled to deep sequencing (ChIP-seq) (Table **EV2**). *De novo* motif finding  
12 identified the consensus CCCCTCCCCC motif in 82.4% of 23756 peaks (Figure **EV3C**), which is  
13 similar to results obtained in Serum/Lif ESCs (Fidalgo *et al*, 2016). Surprisingly, Zfp281 occupancy in  
14 *WT*<sub>2i</sub> and *WT*<sub>32h</sub> cells was as highly correlated (Pearson's correlation coefficient R = 0.81) as between  
15 replicates (R= 0.84 and R=0.85, respectively), with only few peaks exclusively detected in any of the  
16 two cell states (Figure **3E**, **EV3D**). A lower correlation was observed between *WT*<sub>32h</sub> cells and  
17 published data for EpiSCs (Huang *et al*, 2017) (R=0.69) and trophoblast stem cells (TSCs) (Ishiuchi *et*  
18 *al*, 2019) (R=0.55), but binding at peaks associated to cluster 1-6 genes was largely unchanged  
19 (Figure **EV3E**, **F**), suggesting stable chromatin association also during later pluripotency progression  
20 and in lineage-unrelated TSCs. To determine if Zfp281 binds to CREs, we profiled histone H3 lysine  
21 27 acetylation (H3K27ac), a chromatin mark associated with active promoters and enhancers.  
22 Comparison of our Zfp281 and H3K27ac with published histone mark ChIP-seq data (Kurimoto *et al*,  
23 2015; Buecker *et al*, 2014) (Figure **EV3G**) identified 7697 Zfp281 peaks proximal to transcriptional  
24 start sites (TSSs), of which 54% were at active promoters (co-localization with H3K27ac and H3K4 tri-  
25 methylation), and 16059 distal Zfp281 peaks of which 62% were at putative enhancers (co-  
26 localization with H3K4 mono-methylation). 38% of the latter were also enriched for H3K27ac,  
27 qualifying them as active enhancers. Notably, peaks with slightly increased Zfp281 binding in *WT*<sub>32h</sub>  
28 cells gained H3K27ac and expression of associated genes during differentiation, while decreased  
29 binding was associated with reduced H3K27ac and transcription (Figure **3F**). Despite stable  
30 occupancy of target sites, quantitative binding changes of Zfp281 at these sites therefore parallel  
31 differences in CRE activity. However, this was similar at peaks linked to Zfp281-insensitive cluster 1/2  
32 and -sensitive cluster 3/4 genes (Figure **3G**), showing that differential binding strength at CREs  
33 correlates with differentiation-specific gene expression, but only partially with transcriptionally  
34 regulated targets.

### 35 **Zfp281 interacts with Ehmt1 and Zic2 during ESC differentiation**

36 Since chromatin occupancy was largely unchanged, we reasoned that Zfp281 may control transcription  
37 through cell state-specific protein interaction partners. To test this, we performed Zfp281  
38 immunoprecipitations (IPs) coupled to semi-quantitative mass spectrometry (MS) in nuclear extracts of  
39 *WT*<sub>2i</sub> and *WT*<sub>40h</sub> cells, including *Zfp281* KO lysates to control for antibody-specificity (Table **EV3**).

1 Stringent selection criteria identified the previously reported interactor Nanog (Fidalgo *et al*, 2012) in  
2 *WT*<sub>2i</sub> cells and several proteins specifically enriched in *WT*<sub>40h</sub> cells (Figure 4A). Strikingly, the latter were  
3 transcriptionally induced and the former repressed during differentiation (Figure 4B), suggesting that  
4 differential binding to Zfp281 may, at least in part, be driven by protein abundance. To determine  
5 functional downstream effectors, we decided to probe genetic interaction of differentiation-specific  
6 interactors with Zfp281 in our conditionally overexpressing ESCs. To this end we depleted selected  
7 binding partners using siRNA transfection, induced Zfp281 by Dox treatment and quantified *Rex1*  
8 reporter distribution after 32h in 2i (Figure 4C). As controls, we included siRNAs targeting Zfp281 itself  
9 and Tcf711. Transfection of Zfp281 but not Tcf711 siRNAs blocked emergence of GFP<sub>low</sub> cells (76%  
10 reduction) (Figure 4C, EV4A), thus confirming suitability for identifying genetic Zfp281 interactors. Of  
11 all candidates tested individually, only knockdown of Ehmt1 and Zic2 reduced the fraction of GFP<sub>low</sub>  
12 cells (34% and 32%, respectively), an effect enhanced by simultaneous depletion of both (63%).  
13 Conversely, conditional overexpression of Ehmt1 and Zic2 in RGd2 ESCs (Figure EV4B, C), similar to  
14 Zfp281, induced downregulation of the *Rex1* reporter in a subset of cells (Figure EV4D). The *de novo*  
15 DNA methyltransferases Dnmt3a and Dnmt3b have overlapping functions during embryogenesis  
16 (Okano *et al*, 1999) and, hence, may act redundantly. However, simultaneous depletion of Dnmt3a and  
17 Dnmt3b by siRNAs or in compound *Dnmt3a/3b* KO cells (Figure EV4E, F) did not impair Zfp281-induced  
18 reporter repression (Figure 4C, EV4G), demonstrating that Zfp281 drives differentiation independent of  
19 Dnmt3a and Dnmt3b.

20 Zic2 is a zinc finger TF that represses poised developmental enhancers in Serum/Lif ESCs (Luo *et al*,  
21 2015). Ehmt1 (GLP) is a methyltransferase that can be found in a complex with Ehmt2 (G9a), which  
22 both mediate mono- and di-methylation of histone H3 lysine 9 (H3K9me1 and H3K9me2) (Tachibana  
23 *et al*, 2005). The genetic interactions in naïve ESCs (Figure 4C) together with the preferential binding  
24 during differentiation observed in both nuclear extracts using IP-MS (Figure 4A) and whole cell lysates  
25 using IP-western blot (Figure EV4H), suggests that Ehmt1 and Zic2 are functional downstream effectors  
26 of Zfp281.

### 27 **Ehmt1 and Zic2 regulate ESC differentiation and reprogramming of EpiSCs**

28 We therefore generated individual and compound *Ehmt1* and *Zic2* KO RGd2 ESCs (Figure EV5A, B).  
29 In contrast to wildtype or *Zic2* KO cells, *Ehmt1* and *Ehmt1/Zic2* KO cells were spindle-shaped (Figure  
30 EV5C) and proliferated slowly (Figure EV5D). They were not arrested at a specific cell cycle stage  
31 (Figure EV5E) and did not exhibit downregulation of the *Rex1* reporter in 2i (Figure EV5F). After 2i  
32 withdrawal for 32h (or 72h), 75% (9%) of *Ehmt1* and 55% (7%) of *Zic2* KO cells maintained GFP  
33 expression, increasing to 90% (35%) in *Ehmt1/Zic2* compound KO cells (Figure EV5F), while 30% (1%)  
34 of cells from untargeted sibling clones (*Zic2* WT and *Ehmt1* WT) were GFP<sub>high</sub>. Correspondingly, 5%,  
35 4% and 12% of *Zic2*, *Ehmt1* and *Ehmt1/Zic2* KO cells retained self-renewal after 72h of differentiation  
36 (Figure 5A). *Ehmt1* and *Ehmt1/Zic2*, but not *Zic2* KO ESCs, were unable to form polarized spheroids  
37 in Matrigel (Figure 5B). Quantification of this effect was similar to *Zfp281* mutants (Figure EV5G). We  
38 therefore conclude that *Ehmt1* is required for polarization and that *Ehmt1* and *Zic2* promote exit from  
39 self-renewal independently of each other.



1 In the absence of *Ehmt1*, H3K9me2 was limited to DAPI-rich speckles (Figure **EV5H**), which is  
2 reminiscent of the depletion of euchromatic H3K9me2 and its enrichment at pericentric heterochromatin  
3 in *Ehmt2* mutants (Tachibana *et al*, 2002). Since exposure to the Ehmt inhibitors A-366 and UNC0642  
4 induced dose-dependent cell lethality (data not shown), we decided to test Ehmt1's enzymatic activity  
5 by expressing specific loss of function alleles in *Ehmt1* KO cells: An Ehmt1 protein with mutations in  
6 the ankyrin domain (*Ehmt1<sub>ank</sub>*), responsible for binding to methylated H3K9 *in vitro* (Collins *et al*, 2008),  
7 reverted nuclear H3K9me2 distribution (Figure **EV5H**) and resistance to *Rex1* downregulation (Figure  
8 **5C, EV5I**) to a similar extent as the wildtype protein did. In contrast, substitutions in the SET domain  
9 (*Ehmt1<sub>NH-LE</sub>*) that perturb Ehmt1 methyltransferase *in vitro* (Tachibana *et al*, 2008) rescued only partially  
10 and a small deletion in the SET domain (*Ehmt1<sub>ΔNHHC</sub>*) that additionally ablates binding to Ehmt2  
11 completely abolished rescue. Therefore, both catalytic activity of Ehmt1 and formation of a larger  
12 methyltransferase protein complex are implicated in ESC transition.

13 Chemical inhibition and knockdown of Ehmt enzymes in somatic cells enhances reprogramming  
14 (Sridharan *et al*, 2013; Rodriguez-Madoz *et al*, 2017; Shi *et al*, 2008). Consistently, depletion of Ehmt1  
15 but also of *Zic2* in 796.4 and O4GIP<sub>GY118F</sub> EpiSCs increased Epi-iPSC formation in the presence of *Gcsf*  
16 (Figure **5D, EV5J**). The effect was modest, but enhanced by the combined knockdown of both. Taken  
17 together these results suggest that Ehmt1 and *Zic2*, similar to *Zfp281*, drive exit from naïve pluripotency  
18 and restrain reprogramming of EpiSCs. Notably, phenotypes induced by co-depletion of *Zic2* and Ehmt1  
19 were weaker than elimination of *Zfp281*, suggesting existence of additional *Zfp281* effectors that may  
20 include other histone modifying complexes (Huang *et al*, 2017; Zhou *et al*, 2017; Ishiuchi *et al*, 2019).

## 21 **Overlapping transcriptional functions of *Zfp281* and *Ehmt1/Zic2***

22 To test if the biochemical and functional interaction with *Zfp281* is reflected in similar transcriptional  
23 outputs, we profiled mRNA expression in *Ehmt1*, *Zic2* and *Ehmt1/Zic2* KO cells in 2i and after 32h of  
24 differentiation (Table **EV2**). Principle component (PC) analysis, including *Zfp281* KO, EpiLC (Buecker  
25 *et al*, 2014) and EpiSC (Bao *et al*, 2018) datasets, of changes relative to *WT* ESCs identified PC1 to  
26 discriminate developmental timing and to separate differentiated cells from ESCs (Figure **6A**). Mutant  
27 and wildtype ESCs projected similarly onto PC1 and expressed pluripotency marker genes at similar  
28 levels (Figure **EV6A**), confirming their naïve identity. PC2, in contrast, segregated *WT* from *Zfp281* and,  
29 in particular, *Ehmt1* KO genotypes. We, indeed, observed 1274 deregulated genes in *Ehmt1<sub>2i</sub>* cells that  
30 were unchanged in *Zfp281<sub>2i</sub>* cells (Figure **EV6B**). These were enriched for homeostatic and cell  
31 adhesion GO terms (Figure **EV6B**) and likely contribute to the cellular and polarization phenotypes in  
32 *Ehmt1* KO cells.

33 Progression of *Zfp281<sub>16h/32h</sub>*, *Ehmt1<sub>32h</sub>* and *Ehmt1/Zic2<sub>32h</sub>* cells along PC1 was impaired when compared  
34 to matching *WT* controls (Figure **6A**), which we also observed in PC analysis using blastocyst  
35 development datasets (Boroviak *et al*, 2015) (Figure **6B**). In fact, alterations in *Ehmt1* and *Zfp281* KO  
36 cells correlated during differentiation (Figure **EV6C**), suggesting similar defects in developmental  
37 transcription. This correlation was not strong ( $R = 0.44$ ), but increased ( $R=0.57$ ) when only considering  
38 cluster 1-6 gene expression (Figure **EV6D**). Although we also noted slight deregulation of clusters 1  
39 and 2, transcriptional defects in clusters 3-6 were similar in *Ehmt1<sub>32h</sub>* and *Zfp281<sub>32h</sub>* cells (Figure **6C**,

1 **D)**. Ehmt2-dependent H3K9 di-methylation is associated with gene silencing (Zylicz *et al*, 2015),  
2 consistent with the majority of genes showing increased RNA levels in *Ehmt1*<sub>2i</sub> cells (Figure **EV6B**).  
3 Nevertheless, 38% of target genes were downregulated. Changes in the absence of *Ehmt1* are  
4 therefore likely consequential to both direct and indirect effects and may also include the contribution  
5 of non-histone Ehmt1 substrates (Sim *et al*, 2017) to transcription.

6 Based on mRNA levels, *Zic2*<sub>32h</sub> cells were not separated from matching control cells (Figure **6A-D**).  
7 This was surprising, since *Zic2* KO cells appeared similarly impaired in exiting self-renewal as *Ehmt1*  
8 KO cells (Figure **5A**). However, loss of *Zic2* in *Ehmt1*<sub>32h</sub> cells enhanced the deregulation of clusters 1-  
9 4 during differentiation (Figure **6D**) and induced a shift along PC1 (Figure **6A, B**). Linear regression  
10 revealed that perturbations in *Ehmt1/Zic2* KO cells were predominantly the sum of alterations in single  
11 mutants rather than synergistic (Figure **EV6E**), implying subtle, but functionally relevant changes in *Zic2*  
12 KO cells. Ehmt1 and *Zic2* therefore regulate transcription independently of each other, aligning with  
13 their additive loss-of-function phenotypes in differentiation and reprogramming (Figure **5A, D**). Taken  
14 together, this analysis demonstrates connected functions of *Zfp281* and Ehmt1/*Zic2* in gene expression  
15 during cell state transition.

#### 16 **Ehmt1 and Zic2 act downstream of Zfp281 on chromatin**

17 To identify direct targets and to explore how those relate to the physical interaction with *Zfp281* in  
18 differentiated cells, we performed *Zic2* and Ehmt1 ChIP-seq, and profiled H3K9me2 as a proxy for  
19 Ehmt1 activity. Due to absence of ChIP-seq compatible Ehmt1 antibodies, we inserted an N-terminal  
20 Flag-Avi tag at both *Ehmt1* alleles in ESCs expressing the BirA biotin ligase (Figure **EV7A**). This did  
21 not perturb exit from self-renewal (Figure **EV7B**), indicating expression of a functional Ehmt1 fusion  
22 protein (Bio-Ehmt1). ChIP-seq using Streptavidin beads identified broad Ehmt1-occupied chromatin  
23 domains that, consistent with an enzyme-substrate-relationship, scaled with H3K9me2 genome-wide  
24 (Figure **EV7C**). To determine overlap with *Zfp281*, we quantified Ehmt1 and H3K9me2 enrichment at  
25 *Zfp281*-bound and matching unbound control windows (see methods for details). Ehmt1 localization at  
26 both sets of regions was unchanged during differentiation or in *Zfp281* KO cells (Figure **EV7D, E**),  
27 indicating that *Zfp281* is not required for Ehmt1 localization on chromatin. In contrast to Ehmt1,  
28 H3K9me2 increased in *WT*<sub>32h</sub> cells and EpiLCs (Kurimoto *et al*, 2015), with a more pronounced increase  
29 at *Zfp281*-occupied loci than control windows (Figure **7A**). To test if these dynamics require *Zfp281*, we  
30 performed immunofluorescence staining which revealed that mutant cells failed to gain H3K9me2 by  
31 32h after 2i withdrawal (Figure **EV7F**). H3K9me2 ChIP-seq in *Zfp281* mutants confirmed that H3K9me2  
32 levels were unaffected in *Zfp281*<sub>2i</sub> cells but did not increase in *Zfp281*<sub>32h</sub> cells (Figure **7A, EV7E**).  
33 Impaired gain of H3K9me2 was observed at both *Zfp281*-bound and -unbound sites, suggesting that  
34 *Zfp281* is a differentiation-specific pervasive activator of Ehmt1 during ESC transition. *Zic2* ChIP-seq  
35 identified 28495 peaks, of which approximately 30% overlapped with *Zfp281* (Figure **7B**). These were  
36 closer to promoters and enriched for H3K27ac compared to *Zic2*-only and *Zfp281*-only peaks (Figure  
37 **EV7G, H**), suggesting co-localization of *Zfp281* and *Zic2* at CREs. In *WT*<sub>32h</sub> cells, *Zic2* increased  
38 predominantly at co-bound peaks (Figure **7B**). Although we noted a general reduction of *Zic2* on  
39 chromatin in *Zfp281* mutants, *Zic2* localization was particularly perturbed at co-bound sites in *Zfp281*<sub>32h</sub>

1 cells (Figure **7B**, **EV7I**). Our findings therefore suggest that Zfp281 engages Ehmt1 and Zic2 during  
2 ESC differentiation through chromatin co-occupancy-dependent and -independent mechanisms.

3 At Zfp281-bound peaks, the gain of H3K9me2 and Zic2 occurred mostly at mutually exclusive sets of  
4 genomic loci with reduced and increased Zfp281 binding during differentiation, respectively (Figure **7C**,  
5 **D**), indicating that these are sites of direct physical interaction that control transcription of nearby genes.  
6 We therefore stratified H3K9me2 and Zic2 binding dynamics at Zfp281 peaks by gene cluster  
7 association. H3K9me2 increased predominantly at peaks linked to repressed clusters 1 and 3, and Zic2  
8 at peaks belonging to induced clusters 2 and 4 (Figure **7E**). Surprisingly, the gain in *WT*<sub>32h</sub> cells and  
9 reduction in *Zfp281*<sub>32h</sub> cells was indistinguishable between clusters 1 and 3 (for H3K9me2) and clusters  
10 2 and 4 (for Zic2). Hence, Zfp281 catalyzes H3K9me2 and Zic2 deposition at transition-associated  
11 CREs genome-wide and without any qualitative or quantitative specificity for its transcriptional targets  
12 in clusters 3 and 4. Why cluster 1 and 2 gene expression is insensitive to perturbation of H3K9me2 and  
13 Zic2 dynamics in *Zfp281* KO cells (Figure **3C**, **7E**) remains to be determined. Additional chromatin  
14 regulators may be involved, since transcription of clusters 1 and 2 is also less sensitive to *Ehmt1*  
15 depletion than of clusters 3 and 4 (Figure **6D**). We therefore propose that Zfp281 drives and stabilizes  
16 transition-specific transcription, at least in part, through activation of Ehmt1 at cluster 3 CREs and  
17 recruitment or stabilization of Zic2 at cluster 4 CREs.

## 18 19 **DISCUSSION**

20 Cellular plasticity in response to injury *in vivo* or TF overexpression *in vitro* is frequently accompanied  
21 by the reversal of cellular specialization (Merrell & Stanger, 2016). Although single cell profiling has  
22 shown that this process is not a strict inversion of natural development (Gerber *et al*, 2018; Treutlein *et*  
23 *al*, 2016), differentiation and de-differentiation trajectories may mechanistically intersect. We aimed to  
24 uncover such plasticity regulators in pluripotent cells and performed loss-of-function screening for  
25 genes that both drive exit from ESC self-renewal, and shield EpiSCs from reprogramming into the  
26 pluripotent ground state. Within the experimental limitations of this approach we identified only one  
27 gene, the TF *Zfp281*. Such exclusivity suggests a prominent role in establishing and maintaining the  
28 unidirectionality of pluripotent cell state progression *in vitro*. The former is consistent with perturbed  
29 epiblast maturation in *Zfp281* mutant embryos (Huang *et al*, 2017), but if Zfp281 protects cellular  
30 identities against de-differentiation *in vivo* remains to be determined. We, however, note that Zfp281  
31 restrains iPSC formation from fibroblasts at a late pre-iPSC stage (Fidalgo *et al*, 2012), supporting the  
32 notion that resetting of EpiSCs into naïve pluripotency recapitulates a late phase of somatic cell  
33 reprogramming (Dunn *et al*, 2019). Other factors that, similar to Zfp281, drive differentiation and inhibit  
34 de-differentiation of cell states not represented in our ESC-EpiSC conversion system are likely to exist.  
35 We showed that Zfp281 is important for robust ESC differentiation. This is reminiscent of lineage-  
36 specifying TFs, that are specifically expressed in the lineages they instruct (Graf & Enver, 2009). In  
37 adult mice, Zfp281 is indeed transcribed strongest in heart tissue and its overexpression in fibroblasts  
38 enhances cardiac reprogramming (Zhou *et al*, 2017). During ESC differentiation, however, Zfp281  
39 neither changes expression nor occupies distinct genomic sites, indicating a facilitating, rather than

1 specifying, function. Using biochemical, genetic and genomic experiments we provide evidence that  
2 Zfp281 directs sequential gene expression through permissive and instructive mechanisms involving  
3 physical interaction with Ehmt1 and Zic2. Cluster 5 and 6 genes are differentially expressed in EpiSCs,  
4 but transcriptionally primed by Zfp281 throughout differentiation, including in the naïve pluripotent  
5 starting cell state. Cluster 5 contains modulators of cell adhesion that may contribute to polarization of  
6 post-implantation epiblast cells. However, although *Zfp281* null embryos degenerate during  
7 gastrulation, they do form an epithelial egg cylinder (Huang *et al*, 2017), suggesting operation of  
8 compensatory mechanisms *in vivo*. Cluster 3 and 4 genes are, in contrast, regulated by Zfp281  
9 predominantly during transition, enriched for developmental functions, and, therefore, likely responsible  
10 for extinguishing ESC identity. Strikingly, Zfp281 quantitatively decreases at CREs associated with  
11 repressed cluster 3 genes and, *vice versa*, increases at CREs associated with induced cluster 4 genes.  
12 Concomitant gain of H3K9me2 and Zic2 at cluster 3 and 4 CREs, respectively, suggests that subtle  
13 Zfp281 chromatin binding differences are converted into CRE activity changes by reciprocal activation  
14 of Ehmt1 and Zic2. Consistently, embryonic arrest in *Ehmt1* and *Ehmt2* mutant mouse embryos  
15 (Tachibana *et al*, 2002; 2005) has been attributed to reduced H3K9me2 deposition at and impaired  
16 silencing of developmental enhancers (Zylicz *et al*, 2015), while Zic2 triggers neural plate gene  
17 expression in EpiSCs through enhancer activation (Iwafuchi-Doi *et al*, 2012). The molecular  
18 mechanisms inducing differential binding of Zfp281 to Ehmt1 and Zic2 remain to be elucidated. Because  
19 of similar overexpression phenotypes in ESCs we surmise that protein ratios are rate-determining. Zic2  
20 protein levels, despite unchanged mRNA (Figure 4B), indeed increase during differentiation, while  
21 Ehmt1 persists (Figure EV4H). However, Ehmt1 and Ehmt2 interact with additional zinc finger TFs  
22 (Shinkai & Tachibana, 2011) that may compete with Zfp281 for binding to Ehmt1 specifically in ground  
23 state ESCs. Taken together, we suggest that Zfp281 promotes stable cell state transition by  
24 permissively marking cluster 5 and 6 genes for forthcoming developmental regulation, and instructing  
25 cluster 3 and 4 gene expression for elimination of naïve pluripotency, the latter through differential  
26 engagement with Ehmt1 or Zic2 at CREs.

27 Zfp281 drives differentiation to and inhibits reprogramming of EpiSCs, and therefore qualifies as a  
28 bidirectional cell state regulator with antipodal functions during developmental progression and  
29 reversion. If this is because Zfp281-Ehmt1/Zic2 control the same cell state transition and act through  
30 the same target genes in mutual directions remains to be determined. We showed that *Zfp281* KO cells  
31 exposed to differentiation-promoting conditions are less clonogenic than ESCs and give rise to an  
32 equilibrium of Rex1<sup>high</sup> and Rex1<sup>low</sup> cell states that features defective coupling of Rex1 downregulation  
33 with exit from self-renewal. It is therefore conceivable that Zfp281 acts after an initial commitment step  
34 to induce and stabilize irreversible silencing of naïve identity. During reprogramming, Zfp281 may  
35 inversely antagonize induction of naïve pluripotency prior to formation of a Rex1<sup>high</sup> state, which has  
36 recently been shown to mark transition intermediates with full ESC self-renewal activity and destined to  
37 give rise to Epi-iPSCs (Stuart *et al*, 2019). Acting at a late stage of reprogramming also reconciles our  
38 finding of Zfp281 impairing Epi-iPSC formation by STAT3 activation and *Esrrb* overexpression (Figure  
39 1G, EV1F) with the notion that both regimes proceed along distinct transcriptional trajectories before  
40 converging on a Rex1<sup>high</sup> cell state (Stuart *et al*, 2019). However, Zfp281 depletion in EpiSCs also

1 causes cell cycle arrest and apoptosis (Fidalgo *et al*, 2016), but not upregulation of naïve pluripotent  
2 TFs such as Nanog (Figure **EV20**), and is not alone sufficient for reprogramming to Epi-iPSCs in the  
3 presence of 2i (Figure **1F**). Zfp281 activates transcription of Nodal signaling components, such as the  
4 cluster 5 genes *Lefty1* and *Lefty2*, in ESCs, EpiSCs and the post-implantation epiblast (Huang *et al*,  
5 2017). Nodal signaling is required for EpiSC maintenance (Vallier *et al*, 2009), but dispensable for exit  
6 from ESC self-renewal (Mulas *et al*, 2017) and somatic cell reprogramming (Ruetz *et al*, 2017). We  
7 therefore speculate that Zfp281 controls the EpiSC state and reprogramming through different effector  
8 genes. The former through regulation of cluster 5/6 genes, e.g. *Lefty1*, *Lefty2* or cell polarity regulators,  
9 and the latter through stabilization of cell state transition-specific cluster 3/4 genes.

10 In metastable Serum/Lif ESCs, Zfp281 is reported to promote DNA methylation and differentiation by  
11 recruiting Tet1 and silencing Tet2 (Fidalgo *et al*, 2016). Upon exit from the naïve ESC state, Zfp281  
12 binds to Dnmt3a, Dnmt3b and Dnmt3l (Figure **4A**), suggesting that Zfp281 controls 5-methylcytosine  
13 turnover through regulating DNA methylating and demethylating enzymes. Furthermore, Dnmt1,  
14 Dnmt3a and Dnmt3b interact with the Ehmt1-Ehmt2 heterodimer (Epsztejn-Litman *et al*, 2008; Estève  
15 *et al*, 2006), H3K9me2 and 5-methylcytosine marks overlap genome-wide (Meyenn *et al*, 2016) and  
16 DNA is hypomethylated upon depletion or catalytic inhibition of Ehmt2 in ESCs (Zhang *et al*, 2016b).  
17 We, however, showed that Zfp281 drives exit from naïve pluripotency independent of Dnmt3a, Dnmt3b,  
18 Tet1 and Tet2. Although the specific contributions of 5-methylcytosine, H3K9me2, and other Ehmt  
19 substrates (Sim *et al*, 2017) to pluripotent cell plasticity remain to be determined, our findings suggest  
20 that resolution of naïve pluripotency *in vitro* is masked or mechanistically distinct in heterogeneous  
21 Serum/Lif ESC cultures. Similarly, Zic2 has previously been reported to act as a repressor in metastable  
22 Serum/Lif ESCs (Luo *et al*, 2015), but we detect only minor transcriptional defects in naïve *Zic2* KO  
23 ESCs.

24 Using the paradigm of pluripotent cell state conversion *in vitro*, we here identify, in Zfp281, a regulator  
25 of cellular plasticity that modulates CRE activity and transcription without reliance on cell type-restricted  
26 expression or chromatin occupancy. We propose that the persistence of Zfp281 at developmental CREs  
27 throughout cell state transition provides a molecular platform for ordered remodeling of the cis-  
28 regulatory architecture and further consolidation by lineage-specifying TFs. These findings demonstrate  
29 that differential gene expression is not a necessary criterion of cellular plasticity regulators and we  
30 suggest that this feature may not be limited to pluripotent cells.

1 **ACKNOWLEDGMENTS**

2 We would like to thank S. Dessus-Babus, K. Jacobeit, E. Pandini Figueiredo Moreno, T. Roloff and S.  
3 Smallwood (FMI) for processing sequencing samples; L. Gelman, S. Bourke and M. Zinner (FMI) for  
4 imaging assistance; H. Kohler (FMI) for cell sorting; M. Flemr and P. Knuckles (FMI) for advice on  
5 genome editing and CHIP; and P.A. Ginno, L. Hoerner and A.H.F.M. Peters (FMI) for providing reagents.  
6 We are grateful to S. Gasser, M. Michalski, F. Mohn and A.H.F.M. Peters (FMI), and S. Stricker  
7 (Helmholtz Centre) for comments on the manuscript. This work was supported by the EU Seventh  
8 Framework Programme Integrated Project SyBoSS (to A.S. and F.B.) and the Novartis Research  
9 Foundation (to J.B.). A.S is a Medical Research Council Professor.

10

11 **AUTHOR CONTRIBUTIONS**

12 D.M., M.R. and J.B. performed experiments. D.M. and M.B.S. performed bioinformatical analysis, D.H.  
13 mass spectrometry, and I.L. spheroid image analysis. M.W., A.S. and F.B. assisted the esiRNA screen.  
14 D.M. and J.B. wrote the paper.

15

16 **CONFLICT OF INTERESTS**

17 The authors declare no conflict of interests

## 1 REFERENCES

- 2 Acampora D, Di Giovannantonio LG & Simeone A (2013) Otx2 is an intrinsic determinant of the  
3 embryonic stem cell state and is required for transition to a stable epiblast stem cell condition.  
4 *Development* **140**: 43–55
- 5 Acloque H, Adams MS, Fishwick K, Bronner-Fraser M & Nieto MA (2009) Epithelial-mesenchymal  
6 transitions: the importance of changing cell state in development and disease. *J. Clin. Invest.* **119**:  
7 1438–1449
- 8 Amlani B, Liu Y, Chen T, Ee L-S, Lopez P, Heguy A, Apostolou E, Kim SY & Stadtfeld M (2018)  
9 Nascent Induced Pluripotent Stem Cells Efficiently Generate Entirely iPSC-Derived Mice while  
10 Expressing Differentiation-Associated Genes. *Cell Rep* **22**: 876–884
- 11 Bao S, Tang WW, Wu B, Kim S, Li J, Li L, Kobayashi T, Lee C, Chen Y, Wei M, Li S, Dietmann S,  
12 Tang F, Li X & Surani MA (2018) Derivation of hypermethylated pluripotent embryonic stem cells with  
13 high potency. *Cell Res.* **28**: 22–34
- 14 Betschinger J, Nichols J, Dietmann S, Corrin PD, Paddison PJ & Smith A (2013) Exit from  
15 pluripotency is gated by intracellular redistribution of the bHLH transcription factor Tfe3. *Cell* **153**:  
16 335–347
- 17 Boroviak T, Loos R, Bertone P, Smith A & Nichols J (2014) The ability of inner-cell-mass cells to self-  
18 renew as embryonic stem cells is acquired following epiblast specification. *Nat. Cell Biol.* **16**: 516–528
- 19 Boroviak T, Loos R, Lombard P, Okahara J, Behr R, Sasaki E, Nichols J, Smith A & Bertone P (2015)  
20 Lineage-Specific Profiling Delineates the Emergence and Progression of Naive Pluripotency in  
21 Mammalian Embryogenesis. *Dev. Cell* **35**: 366–382
- 22 Brons IGM, Smithers LE, Trotter MWB, Rugg-Gunn P, Sun B, Chuva de Sousa Lopes SM, Howlett  
23 SK, Clarkson A, Ahrlund-Richter L, Pedersen RA & Vallier L (2007) Derivation of pluripotent epiblast  
24 stem cells from mammalian embryos. *Nature* **448**: 191–195
- 25 Buckley SM, Aranda-Orgilles B, Strikoudis A, Apostolou E, Loizou E, Moran-Crusio K, Farnsworth CL,  
26 Koller AA, Dasgupta R, Silva JC, Stadtfeld M, Hochedlinger K, Chen EI & Aifantis I (2012) Regulation  
27 of pluripotency and cellular reprogramming by the ubiquitin-proteasome system. *Cell Stem Cell* **11**:  
28 783–798
- 29 Buecker C, Srinivasan R, Wu Z, Calo E, Acampora D, Faial T, Simeone A, Tan M, Swigut T &  
30 Wysocka J (2014) Reorganization of enhancer patterns in transition from naive to primed  
31 pluripotency. *Cell Stem Cell* **14**: 838–853
- 32 Cacchiarelli D, Trapnell C, Ziller MJ, Soumillon M, Cesana M, Karnik R, Donaghey J, Smith ZD,  
33 Ratanasirintrao S, Zhang X, Ho Sui SJ, Wu Z, Akopian V, Gifford CA, Doench J, Rinn JL, Daley  
34 GQ, Meissner A, Lander ES & Mikkelsen TS (2015) Integrative Analyses of Human Reprogramming  
35 Reveal Dynamic Nature of Induced Pluripotency. *Cell* **162**: 412–424
- 36 Collins RE, Northrop JP, Horton JR, Lee DY, Zhang X, Stallcup MR & Cheng X (2008) The ankyrin  
37 repeats of G9a and GLP histone methyltransferases are mono- and dimethyllysine binding modules.  
38 *Nat. Struct. Mol. Biol.* **15**: 245–250
- 39 Ding L, Paszkowski-Rogacz M, Nitzsche A, Slabicki MM, Heninger A-K, de Vries I, Kittler R,  
40 Junqueira M, Shevchenko A, Schulz H, Hübner N, Doss MX, Sachinidis A, Hescheler J, Iacone R,  
41 Anastassiadis K, Stewart AF, Pisabarro MT, Caldarelli A, Poser I, et al (2009) A genome-scale RNAi  
42 screen for Oct4 modulators defines a role of the Paf1 complex for embryonic stem cell identity. *Cell*  
43 *Stem Cell* **4**: 403–415
- 44 Domcke S, Bardet AF, Adrian Ginno P, Hartl D, Burger L & Schübeler D (2015) Competition between  
45 DNA methylation and transcription factors determines binding of NRF1. *Nature* **528**: 575–579

- 1 Dorighi KM, Swigut T, Henriques T, Bhanu NV, Scruggs BS, Nady N, Still CD, Garcia BA, Adelman K  
2 & Wysocka J (2017) Mll3 and Mll4 Facilitate Enhancer RNA Synthesis and Transcription from  
3 Promoters Independently of H3K4 Monomethylation. *Mol. Cell* **66**: 568–576.e4
- 4 Dunn S-J, Li MA, Carbognin E, Smith A & Martello G (2019) A common molecular logic determines  
5 embryonic stem cell self-renewal and reprogramming. *EMBO J.* **38**: e100003
- 6 Ebnet K, Kummer D, Steinbacher T, Singh A, Nakayama M & Matis M (2018) Regulation of cell  
7 polarity by cell adhesion receptors. *Semin. Cell Dev. Biol.* **81**: 2–12
- 8 Epsztejn-Litman S, Feldman N, Abu-Remaileh M, Shufaro Y, Gerson A, Ueda J, Deplus R, Fuks F,  
9 Shinkai Y, Cedar H & Bergman Y (2008) De novo DNA methylation promoted by G9a prevents  
10 reprogramming of embryonically silenced genes. *Nat. Struct. Mol. Biol.* **15**: 1176–1183
- 11 Estève P-O, Chin HG, Smallwood A, Feehery GR, Gangisetty O, Karpf AR, Carey MF & Pradhan S  
12 (2006) Direct interaction between DNMT1 and G9a coordinates DNA and histone methylation during  
13 replication. *Genes Dev.* **20**: 3089–3103
- 14 Factor DC, Corradin O, Zentner GE, Saiakhova A, Song L, Chenoweth JG, McKay RD, Crawford GE,  
15 Scacheri PC & Tesar PJ (2014) Epigenomic comparison reveals activation of ‘seed’ enhancers during  
16 transition from naive to primed pluripotency. *Cell Stem Cell* **14**: 854–863
- 17 Festuccia N, Osorno R, Halbritter F, Karwacki-Neisius V, Navarro P, Colby D, Wong F, Yates A,  
18 Tomlinson SR & Chambers I (2012) Esrrb is a direct Nanog target gene that can substitute for Nanog  
19 function in pluripotent cells. *Cell Stem Cell* **11**: 477–490
- 20 Fidalgo M, Faiola F, Pereira C-F, Ding J, Saunders A, Gingold J, Schaniel C, Lemischka IR, Silva  
21 JCR & Wang J (2012) Zfp281 mediates Nanog autorepression through recruitment of the NuRD  
22 complex and inhibits somatic cell reprogramming. *Proc. Natl. Acad. Sci. U.S.A.* **109**: 16202–16207
- 23 Fidalgo M, Huang X, Guallar D, Sanchez-Priego C, Valdes VJ, Saunders A, Ding J, Wu W-S, Clavel  
24 C & Wang J (2016) Zfp281 Coordinates Opposing Functions of Tet1 and Tet2 in Pluripotent States.  
25 *Cell Stem Cell* **19**: 355–369
- 26 Gaidatzis D, Lerch A, Hahne F & Stadler MB (2015) QuasR: quantification and annotation of short  
27 reads in R. *Bioinformatics* **31**: 1130–1132
- 28 Gaujoux R & Seoighe C (2010) A flexible R package for nonnegative matrix factorization. *BMC*  
29 *Bioinformatics* **11**: 367
- 30 Gerber T, Murawala P, Knapp D, Masselink W, Schuez M, Hermann S, Gac-Santel M, Nowoshilow S,  
31 Kageyama J, Khattak S, Currie J, Camp JG, Tanaka EM & Treutlein B (2018) Single-cell analysis  
32 uncovers convergence of cell identities during axolotl limb regeneration. *Science* **362**: eaaq0681
- 33 Graf T & Enver T (2009) Forcing cells to change lineages. *Nature* **462**: 587–594
- 34 Gu Z, Eils R & Schlesner M (2016) Complex heatmaps reveal patterns and correlations in  
35 multidimensional genomic data. *Bioinformatics* **32**: 2847–2849
- 36 Guo G, Huang Y, Humphreys P, Wang X & Smith A (2011) A PiggyBac-based recessive screening  
37 method to identify pluripotency regulators. *PLoS ONE* **6**: e18189
- 38 Guo G, Yang J, Nichols J, Hall JS, Eyres I, Mansfield W & Smith A (2009) Klf4 reverts  
39 developmentally programmed restriction of ground state pluripotency. *Development* **136**: 1063–1069
- 40 Hayashi K, Ohta H, Kurimoto K, Aramaki S & Saitou M (2011) Reconstitution of the mouse germ cell  
41 specification pathway in culture by pluripotent stem cells. *Cell* **146**: 519–532



- 1 Huang DW, Sherman BT & Lempicki RA (2009) Bioinformatics enrichment tools: paths toward the  
2 comprehensive functional analysis of large gene lists. *Nucleic Acids Res.* **37**: 1–13
- 3 Huang X, Balmer S, Yang F, Fidalgo M, Li D, Guallar D, Hadjantonakis A-K & Wang J (2017) Zfp281  
4 is essential for mouse epiblast maturation through transcriptional and epigenetic control of Nodal  
5 signaling. *Elife* **6**: 243
- 6 Ishiuchi T, Ohishi H, Sato T, Kamimura S, Yorino M, Abe S, Suzuki A, Wakayama T, Suyama M &  
7 Sasaki H (2019) Zfp281 Shapes the Transcriptome of Trophoblast Stem Cells and Is Essential for  
8 Placental Development. *Cell Rep* **27**: 1742–1754.e6
- 9 Iwafuchi-Doi M, Matsuda K, Murakami K, Niwa H, Tesar PJ, Aruga J, Matsuo I & Kondoh H (2012)  
10 Transcriptional regulatory networks in epiblast cells and during anterior neural plate development as  
11 modeled in epiblast stem cells. *Development* **139**: 3926–3937
- 12 Jackson SA, Olufs ZPG, Tran KA, Zaidan NZ & Sridharan R (2016) Alternative Routes to Induced  
13 Pluripotent Stem Cells Revealed by Reprogramming of the Neural Lineage. *Stem Cell Reports* **6**:  
14 302–311
- 15 Kalkan T, Olova N, Roode M, Mulas C, Lee HJ, Nett I, Marks H, Walker R, Stunnenberg HG, Lilley  
16 KS, Nichols J, Reik W, Bertone P & Smith A (2017) Tracking the embryonic stem cell transition from  
17 ground state pluripotency. *Development* **144**: 1221–1234
- 18 Kojima Y, Kaufman-Francis K, Studdert JB, Steiner KA, Power MD, Loebel DAF, Jones V, Hor A, de  
19 Alencastro G, Logan GJ, Teber ET, Tam OH, Stutz MD, Alexander IE, Pickett HA & Tam PPL (2014)  
20 The transcriptional and functional properties of mouse epiblast stem cells resemble the anterior  
21 primitive streak. *Cell Stem Cell* **14**: 107–120
- 22 Kurimoto K, Yabuta Y, Hayashi K, Ohta H, Kiyonari H, Mitani T, Moritoki Y, Kohri K, Kimura H,  
23 Yamamoto T, Katou Y, Shirahige K & Saitou M (2015) Quantitative Dynamics of Chromatin  
24 Remodeling during Germ Cell Specification from Mouse Embryonic Stem Cells. *Cell Stem Cell* **16**:  
25 517–532
- 26 Ladewig J, Koch P & Brüstle O (2013) Leveling Waddington: the emergence of direct programming  
27 and the loss of cell fate hierarchies. *Nat. Rev. Mol. Cell Biol.* **14**: 225–236
- 28 Langmead B, Trapnell C, Pop M & Salzberg SL (2009) Ultrafast and memory-efficient alignment of  
29 short DNA sequences to the human genome. *Genome Biol.* **10**: R25
- 30 Lawrence M, Huber W, Pagès H, Aboyoun P, Carlson M, Gentleman R, Morgan MT & Carey VJ  
31 (2013) Software for computing and annotating genomic ranges. *PLoS Comput. Biol.* **9**: e1003118
- 32 Leeb M, Dietmann S, Paramor M, Niwa H & Smith A (2014) Genetic exploration of the exit from self-  
33 renewal using haploid embryonic stem cells. *Cell Stem Cell* **14**: 385–393
- 34 Levine JH, Simonds EF, Bendall SC, Davis KL, Amir E-AD, Tadmor MD, Litvin O, Fienberg HG, Jager  
35 A, Zunder ER, Finck R, Gedman AL, Radtke I, Downing JR, Pe'er D & Nolan GP (2015) Data-Driven  
36 Phenotypic Dissection of AML Reveals Progenitor-like Cells that Correlate with Prognosis. *Cell* **162**:  
37 184–197
- 38 Li M, Yu JSL, Tilgner K, Ong SH, Koike-Yusa H & Yusa K (2018) Genome-wide CRISPR-KO Screen  
39 Uncovers mTORC1-Mediated Gsk3 Regulation in Naive Pluripotency Maintenance and Dissolution.  
40 *Cell Rep* **24**: 489–502
- 41 Li R, Liang J, Ni S, Zhou T, Qing X, Li H, He W, Chen J, Li F, Zhuang Q, Qin B, Xu J, Li W, Yang J,  
42 Gan Y, Qin D, Feng S, Song H, Yang D, Zhang B, et al (2010) A mesenchymal-to-epithelial transition  
43 initiates and is required for the nuclear reprogramming of mouse fibroblasts. *Cell Stem Cell* **7**: 51–63

- 1 Luo Z, Gao X, Lin C, Smith ER, Marshall SA, Swanson SK, Florens L, Washburn MP & Shilatifard A  
2 (2015) Zic2 is an enhancer-binding factor required for embryonic stem cell specification. *Mol. Cell* **57**:  
3 685–694
- 4 Mali P, Yang L, Esvelt KM, Aach J, Guell M, DiCarlo JE, Norville JE & Church GM (2013) RNA-guided  
5 human genome engineering via Cas9. *Science* **339**: 823–826
- 6 Martello G, Sugimoto T, Diamanti E, Joshi A, Hannah R, Ohtsuka S, Göttgens B, Niwa H & Smith A  
7 (2012) Esrrb is a pivotal target of the Gsk3/Tcf3 axis regulating embryonic stem cell self-renewal. *Cell*  
8 *Stem Cell* **11**: 491–504
- 9 Merrell AJ & Stanger BZ (2016) Adult cell plasticity in vivo: de-differentiation and transdifferentiation  
10 are back in style. *Nat. Rev. Mol. Cell Biol.* **17**: 413–425
- 11 Meyenn von F, Iurlaro M, Habibi E, Liu NQ, Salehzadeh-Yazdi A, Santos F, Petrini E, Milagre I, Yu M,  
12 Xie Z, Kroeze LI, Nesterova TB, Jansen JH, Xie H, He C, Reik W & Stunnenberg HG (2016)  
13 Impairment of DNA Methylation Maintenance Is the Main Cause of Global Demethylation in Naive  
14 Embryonic Stem Cells. *Mol. Cell* **62**: 848–861
- 15 Mulas C, Kalkan T & Smith A (2017) NODAL Secures Pluripotency upon Embryonic Stem Cell  
16 Progression from the Ground State. *Stem Cell Reports* **9**: 77–91
- 17 Nefzger CM, Rossello FJ, Chen J, Liu X, Knaupp AS, Firas J, Paynter JM, Pflueger J, Buckberry S,  
18 Lim SM, Williams B, Alaei S, Faye-Chauhan K, Petretto E, Nilsson SK, Lister R, Ramialison M, Powell  
19 DR, Rackham OJL & Polo JM (2017) Cell Type of Origin Dictates the Route to Pluripotency. *Cell Rep*  
20 **21**: 2649–2660
- 21 Niwa H, Ogawa K, Shimosato D & Adachi K (2009) A parallel circuit of LIF signalling pathways  
22 maintains pluripotency of mouse ES cells. *Nature* **460**: 118–122
- 23 Okano M, Bell DW, Haber DA & Li E (1999) DNA methyltransferases Dnmt3a and Dnmt3b are  
24 essential for de novo methylation and mammalian development. *Cell* **99**: 247–257
- 25 Okita Y, Matsumoto A, Yumimoto K, Isoshita R & Nakayama KI (2012) Increased efficiency in the  
26 generation of induced pluripotent stem cells by Fbxw7 ablation. *Genes Cells* **17**: 768–777
- 27 Osorno R, Tsakiridis A, Wong F, Cambray N, Economou C, Wilkie R, Blin G, Scotting PJ, Chambers I  
28 & Wilson V (2012) The developmental dismantling of pluripotency is reversed by ectopic Oct4  
29 expression. *Development* **139**: 2288–2298
- 30 Ostapczuk V, Mohn F, Carl SH, Basters A, Hess D, Iesmantavicius V, Lampersberger L, Flemr M,  
31 Pandey A, Thomä NH, Betschinger J & Bühler M (2018) Activity-dependent neuroprotective protein  
32 recruits HP1 and CHD4 to control lineage-specifying genes. *Nature* **557**: 739–743
- 33 Pereira L, Yi F & Merrill BJ (2006) Repression of Nanog gene transcription by Tcf3 limits embryonic  
34 stem cell self-renewal. *Mol. Cell. Biol.* **26**: 7479–7491
- 35 Raab S, Klingenstein M, Möller A, Illing A, Tosic J, Breunig M, Kuales G, Linta L, Seufferlein T, Arnold  
36 SJ, Kleger A & Liebau S (2017) Reprogramming to pluripotency does not require transition through a  
37 primitive streak-like state. *Sci Rep* **7**: 16543
- 38 Rais Y, Zviran A, Geula S, Gafni O, Chomsky E, Viukov S, Mansour AA, Caspi I, Krupalnik V, Zerbib  
39 M, Maza I, Mor N, Baran D, Weinberger L, Jaitin DA, Lara-Astiaso D, Blecher-Gonen R, Shipony Z,  
40 Mukamel Z, Hagai T, et al (2013) Deterministic direct reprogramming of somatic cells to pluripotency.  
41 *Nature* **502**: 65–70
- 42 Ritchie ME, Phipson B, Wu D, Hu Y, Law CW, Shi W & Smyth GK (2015) limma powers differential  
43 expression analyses for RNA-sequencing and microarray studies. *Nucleic Acids Res.* **43**: e47–e47

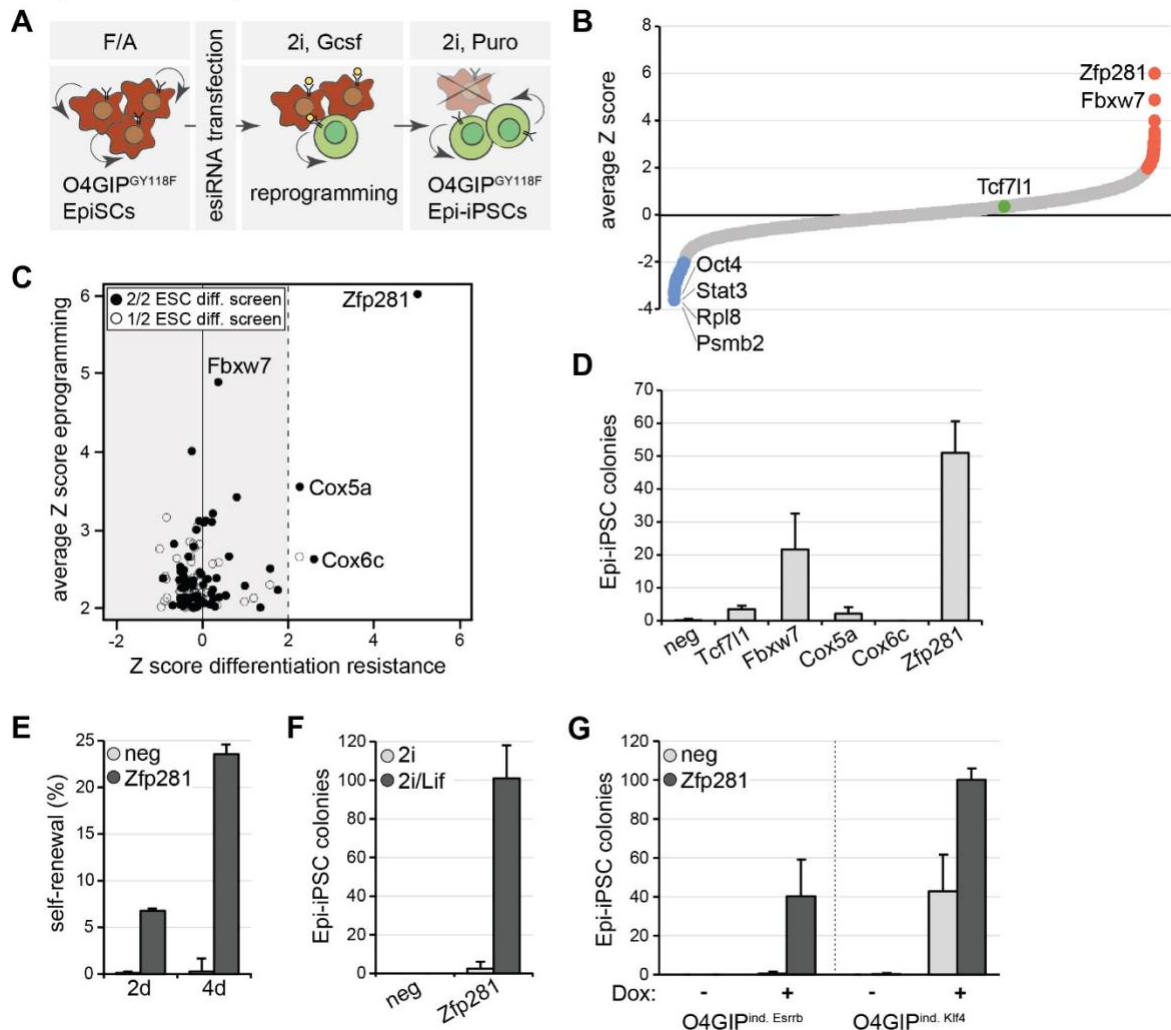
- 1 Robinson MD & Oshlack A (2010) A scaling normalization method for differential expression analysis  
2 of RNA-seq data. *Genome Biol.* **11**: R25
- 3 Rodriguez-Madoz JR, San Jose-Eneriz E, Rabal O, Zapata-Linares N, Miranda E, Rodriguez S,  
4 Porciuncula A, Vilas-Zornoza A, Garate L, Segura V, Guruceaga E, Agirre X, Oyarzabal J & Prosper  
5 F (2017) Reversible dual inhibitor against G9a and DNMT1 improves human iPSC derivation  
6 enhancing MET and facilitating transcription factor engagement to the genome. *PLoS ONE* **12**:  
7 e0190275
- 8 Ruetz T, Pfisterer U, Di Stefano B, Ashmore J, Beniazza M, Tian TV, Kaemena DF, Tosti L, Tan W,  
9 Manning JR, Chantzoura E, Ottosson DR, Collombet S, Johnsson A, Cohen E, Yusa K, Linnarsson S,  
10 Graf T, Parmar M & Kaji K (2017) Constitutively Active SMAD2/3 Are Broad-Scope Potentiators of  
11 Transcription-Factor-Mediated Cellular Reprogramming. *Cell Stem Cell* **21**: 791–805.e9
- 12 Samavarchi-Tehrani P, Golipour A, David L, Sung H-K, Beyer TA, Datti A, Woltjen K, Nagy A &  
13 Wrana JL (2010) Functional genomics reveals a BMP-driven mesenchymal-to-epithelial transition in  
14 the initiation of somatic cell reprogramming. *Cell Stem Cell* **7**: 64–77
- 15 Shahbazi MN, Scialdone A, Skorupska N, Weberling A, Recher G, Zhu M, Jedrusik A, Devito LG, Noli  
16 L, Macaulay IC, Buecker C, Khalaf Y, Ilic D, Voet T, Marioni JC & Zernicka-Goetz M (2017)  
17 Pluripotent state transitions coordinate morphogenesis in mouse and human embryos. *Nature* **552**:  
18 239–243
- 19 Shi Y, Desponts C, Do JT, Hahm HS, Schöler HR & Ding S (2008) Induction of pluripotent stem cells  
20 from mouse embryonic fibroblasts by Oct4 and Klf4 with small-molecule compounds. *Cell Stem Cell*  
21 **3**: 568–574
- 22 Shinkai Y & Tachibana M (2011) H3K9 methyltransferase G9a and the related molecule GLP. *Genes*  
23 *Dev.* **25**: 781–788
- 24 Sim Y-J, Kim M-S, Nayfeh A, Yun Y-J, Kim S-J, Park K-T, Kim C-H & Kim K-S (2017) 2i Maintains a  
25 Naive Ground State in ESCs through Two Distinct Epigenetic Mechanisms. *Stem Cell Reports* **8**:  
26 1312–1328
- 27 Smith A (2017) Formative pluripotency: the executive phase in a developmental continuum.  
28 *Development* **144**: 365–373
- 29 Sridharan R, Gonzales-Cope M, Chronis C, Bonora G, McKee R, Huang C, Patel S, Lopez D, Mishra  
30 N, Pellegrini M, Carey M, Garcia BA & Plath K (2013) Proteomic and genomic approaches reveal  
31 critical functions of H3K9 methylation and heterochromatin protein-1γ in reprogramming to  
32 pluripotency. *Nat. Cell Biol.* **15**: 872–882
- 33 Stuart HT, Stirparo GG, Lohoff T, Bates LE, Kinoshita M, Lim CY, Sousa EJ, Maskalenka K,  
34 Radzishchenskaya A, Malcolm AA, Alves MRP, Lloyd RL, Nestorowa S, Humphreys P, Mansfield W,  
35 Reik W, Bertone P, Nichols J, Göttgens B & Silva JCR (2019) Distinct Molecular Trajectories  
36 Converge to Induce Naive Pluripotency. *Cell Stem Cell* **25**: 388–406
- 37 Tachibana M, Matsumura Y, Fukuda M, Kimura H & Shinkai Y (2008) G9a/GLP complexes  
38 independently mediate H3K9 and DNA methylation to silence transcription. *EMBO J.* **27**: 2681–  
39 2690
- 40 Tachibana M, Sugimoto K, Nozaki M, Ueda J, Ohta T, Ohki M, Fukuda M, Takeda N, Niida H, Kato H  
41 & Shinkai Y (2002) G9a histone methyltransferase plays a dominant role in euchromatic histone  
42 H3 lysine 9 methylation and is essential for early embryogenesis. *Genes Dev.* **16**: 1779–1791
- 43 Tachibana M, Ueda J, Fukuda M, Takeda N, Ohta T, Iwanari H, Sakihama T, Kodama T, Hamakubo  
44 T & Shinkai Y (2005) Histone methyltransferases G9a and GLP form heteromeric complexes and  
45 are both crucial for methylation of euchromatin at H3-K9. *Genes Dev.* **19**: 815–826

- 1 Takahashi K & Yamanaka S (2006) Induction of pluripotent stem cells from mouse embryonic and  
2 adult fibroblast cultures by defined factors. *Cell* **126**: 663–676
- 3 Takahashi K & Yamanaka S (2015) A developmental framework for induced pluripotency.  
4 *Development* **142**: 3274–3285
- 5 Takahashi K, Tanabe K, Ohnuki M, Narita M, Sasaki A, Yamamoto M, Nakamura M, Sutou K,  
6 Osafune K & Yamanaka S (2014) Induction of pluripotency in human somatic cells via a transient  
7 state resembling primitive streak-like mesendoderm. *Nat Commun* **5**: 3678
- 8 Tesar PJ, Chenoweth JG, Brook FA, Davies TJ, Evans EP, Mack DL, Gardner RL & McKay RDG  
9 (2007) New cell lines from mouse epiblast share defining features with human embryonic stem  
10 cells. *Nature* **448**: 196–199
- 11 Treutlein B, Lee QY, Camp JG, Mall M, Koh W, Shariati SAM, Sim S, Neff NF, Skotheim JM, Wernig  
12 M & Quake SR (2016) Dissecting direct reprogramming from fibroblast to neuron using single-cell  
13 RNA-seq. *Nature* **534**: 391–395
- 14 Tsakiridis A, Huang Y, Blin G, Skylaki S, Wymeersch F, Osorno R, Economou C, Karagianni E, Zhao  
15 S, Lowell S & Wilson V (2014) Distinct Wnt-driven primitive streak-like populations reflect in vivo  
16 lineage precursors. *Development* **141**: 1209–1221
- 17 Vallier L, Mendjan S, Brown S, Chng Z, Teo A, Smithers LE, Trotter MWB, Cho CH-H, Martinez A,  
18 Rugg-Gunn P, Brons G & Pedersen RA (2009) Activin/Nodal signalling maintains pluripotency by  
19 controlling Nanog expression. *Development* **136**: 1339–1349
- 20 Villegas F, Lehalle D, Mayer D, Rittirsch M, Stadler MB, Zinner M, Olivieri D, Vabres P, Duplomb-  
21 Jegu L, De Bont ESJM, Duffourd Y, Duijkers F, Avila M, Geneviève D, Houcinat N, Jouan T,  
22 Kuentz P, Lichtenbelt KD, Thauvin-Robinet C, St-Onge J, et al (2019) Lysosomal Signaling  
23 Licenses Embryonic Stem Cell Differentiation via Inactivation of Tfe3. *Cell Stem Cell* **24**: 257–270
- 24 Wang H, Yang H, Shivalila CS, Dawlaty MM, Cheng AW, Zhang F & Jaenisch R (2013) One-step  
25 generation of mice carrying mutations in multiple genes by CRISPR/Cas-mediated genome  
26 engineering. *Cell* **153**: 910–918
- 27 Westerman BA, Braat AK, Taub N, Potman M, Vissers JHA, Blom M, Verhoeven E, Stoop H, Gillis A,  
28 Velds A, Nijkamp W, Beijersbergen R, Huber LA, Looijenga LHJ & van Lohuizen M (2011) A  
29 genome-wide RNAi screen in mouse embryonic stem cells identifies Mp1 as a key mediator of  
30 differentiation. *J. Exp. Med.* **208**: 2675–2689
- 31 Wray J, Kalkan T, Gomez-Lopez S, Eckardt D, Cook A, Kemler R & Smith A (2011) Inhibition of  
32 glycogen synthase kinase-3 alleviates Tcf3 repression of the pluripotency network and increases  
33 embryonic stem cell resistance to differentiation. *Nat. Cell Biol.* **13**: 838–845
- 34 Yamane M, Ohtsuka S, Matsuura K, Nakamura A & Niwa H (2018) Overlapping functions of Krüppel-  
35 like factor family members: targeting multiple transcription factors to maintain the naïve  
36 pluripotency of mouse embryonic stem cells. *Development* **145**: dev162404
- 37 Yang J, van Oosten AL, Theunissen TW, Guo G, Silva JCR & Smith A (2010) Stat3 activation is  
38 limiting for reprogramming to ground state pluripotency. *Cell Stem Cell* **7**: 319–328
- 39 Zhang H, Gayen S, Xiong J, Zhou B, Shanmugam AK, Sun Y, Karatas H, Liu L, Rao RC, Wang S,  
40 Nesvizhskii AI, Kalantry S & Dou Y (2016a) MLL1 Inhibition Reprograms Epiblast Stem Cells to  
41 Naive Pluripotency. *Cell Stem Cell* **18**: 481–494
- 42 Zhang K, Li L, Huang C, Shen C, Tan F, Xia C, Liu P, Rossant J & Jing N (2010) Distinct functions of  
43 BMP4 during different stages of mouse ES cell neural commitment. *Development* **137**: 2095–  
44 2105

- 1 Zhang T, Termanis A, Özkan B, Bao XX, Culley J, de Lima Alves F, Rappsilber J, Ramsahoye B &  
2 Stancheva I (2016b) G9a/GLP Complex Maintains Imprinted DNA Methylation in Embryonic  
3 Stem Cells. *Cell Rep* **15**: 77–85
- 4 Zhang Y, Liu T, Meyer CA, Eeckhoute J, Johnson DS, Bernstein BE, Nusbaum C, Myers RM, Brown  
5 M, Li W & Liu XS (2008) Model-based analysis of ChIP-Seq (MACS). *Genome Biol.* **9**: R137
- 6 Zhou H, Morales MG, Hashimoto H, Dickson ME, Song K, Ye W, Kim MS, Niederstrasser H, Wang Z,  
7 Chen B, Posner BA, Bassel-Duby R & Olson EN (2017) ZNF281 enhances cardiac  
8 reprogramming by modulating cardiac and inflammatory gene expression. *Genes Dev.* **31**: 1770–  
9 1783
- 10 Zyllicz JJ, Dietmann S, Günesdogan U, Hackett JA, Cougot D, Lee C & Surani MA (2015) Chromatin  
11 dynamics and the role of G9a in gene regulation and enhancer silencing during early mouse  
12 development. *Elife* **4**: 717

1 **MAIN FIGURES**

**Mayer et al., Figure 1**



2

3 **Figure 1: Zfp281 inhibits reprogramming of EpiSCs.**

4 (A) Schematic outline of the reprogramming screen. Red indicates O4GiP<sub>GY118F</sub> EpiSCs and green  
5 O4GIP<sub>GY118F</sub> Epi-iPSCs.

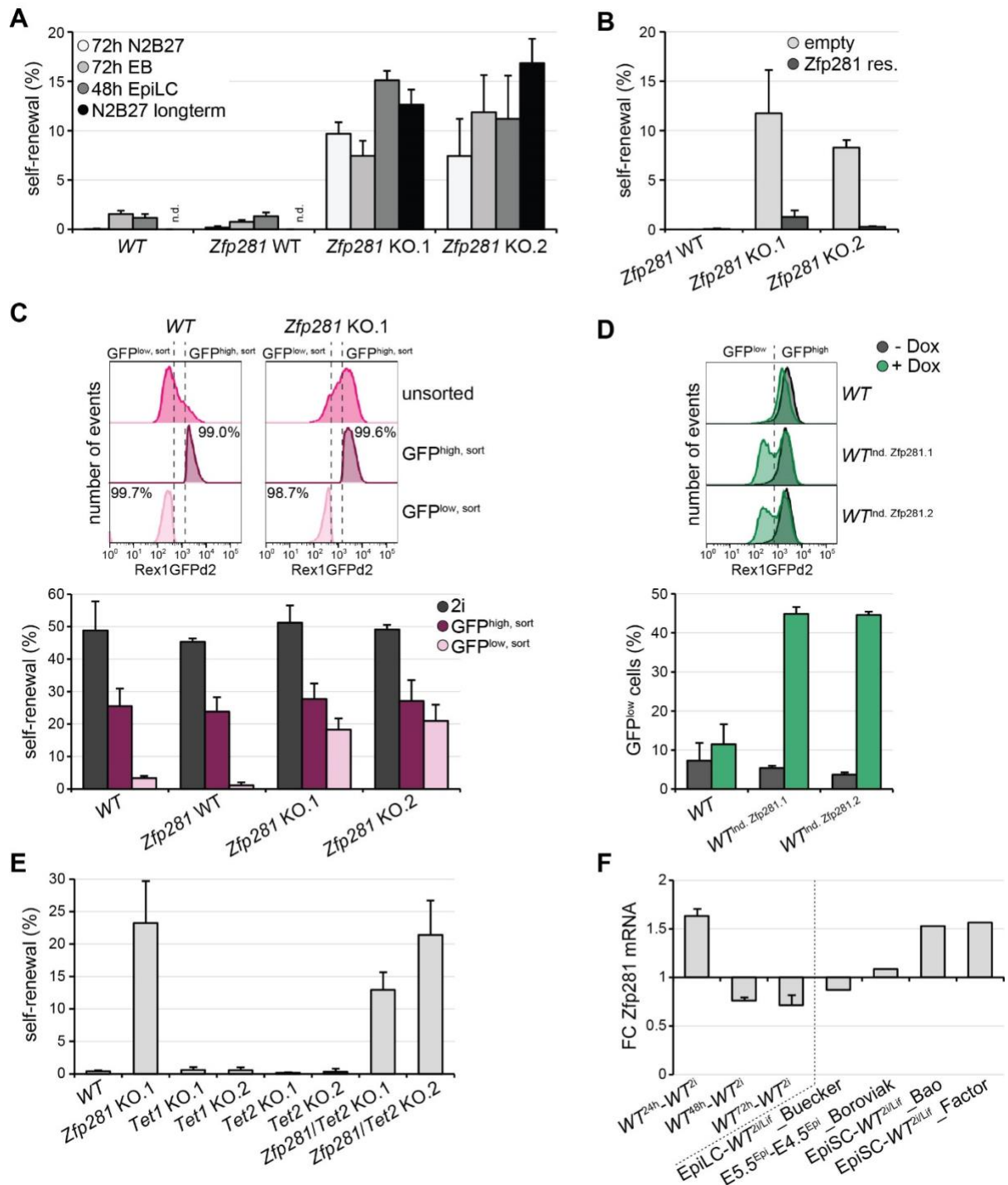
6 (B) Average Z scores of the two screen replicates. Note that esiRNAs targeting *Mll1* (Zhang *et al*,  
7 2016a) and *Mbd3* (Rais *et al*, 2013) were not included in our library and that *Otx2* (Acampora *et al*,  
8 2013) scored below the significance threshold. Screen hits with negative (blue) and positive (red) Z  
9 scores (red), and *Tcf711* (green) are highlighted.

10 (C) Comparison of reprogramming screen hits with two ESC differentiation screens (Betschinger *et al*,  
11 2013; Li *et al*, 2018). Empty and full circles indicate genes recovered in one and both ESC differentiation  
12 screens, respectively.

13 (D) Number of Epi-iPSC colonies derived from 796.4 EpiSCs transfected with indicated siRNAs,  
14 stimulated with Gcsf and 2i for 4d, and selected with Puromycin. Average and standard deviation (SD)  
15 of 3 experiments performed in duplicates. Negative siRNA (neg).

- 1 **(E)** Self-renewal of O4GIP<sub>GY118F</sub> reprogramming intermediates after 2d or 4d of stimulation with Gcsf  
2 and 2i following transfection with indicated siRNAs. Average and SD of 2 experiments performed in  
3 duplicates.
- 4 **(F)** Number of Epi-iPSC colonies derived from OEC2 EpiSCs transfected with indicated siRNAs, treated  
5 for 4d in 2i or 2i/Lif medium, and selected with Puromycin. Average and SD of 2 experiments performed  
6 in duplicates.
- 7 **(G)** Number of Epi-iPSC colonies derived from O4GIP EpiSCs carrying Dox-inducible Esrrb or Klf4  
8 transgenes after transfection with indicated siRNAs, stimulation with or without Dox for 2d, and selection  
9 with Puromycin. Average and SD of 2 experiments performed in duplicates.

## Mayer et al., Figure 2



1

### 2 **Figure 2: Zfp281 drives exit from naïve pluripotency independent of Tet enzymes.**

3 (A, B, E) Self-renewal in RGd2 ESCs of specified genotypes expressing indicated transgenes (B) after  
 4 differentiation in indicated conditions (A) or 72h in N2B27 (B, E). Average and SD of 2 experiments  
 5 performed in duplicates. Note that control cells were lost during continuous passaging in N2B27 (A).  
 6 Not determined (n.d.).

7 (C) Representative flow cytometry profiles of WT and Zfp281 KO.1 cells after 32h of 2i withdrawal  
 8 before (unsorted) and after purification of cells with indicated GFP expression (top panel). Self-renewal

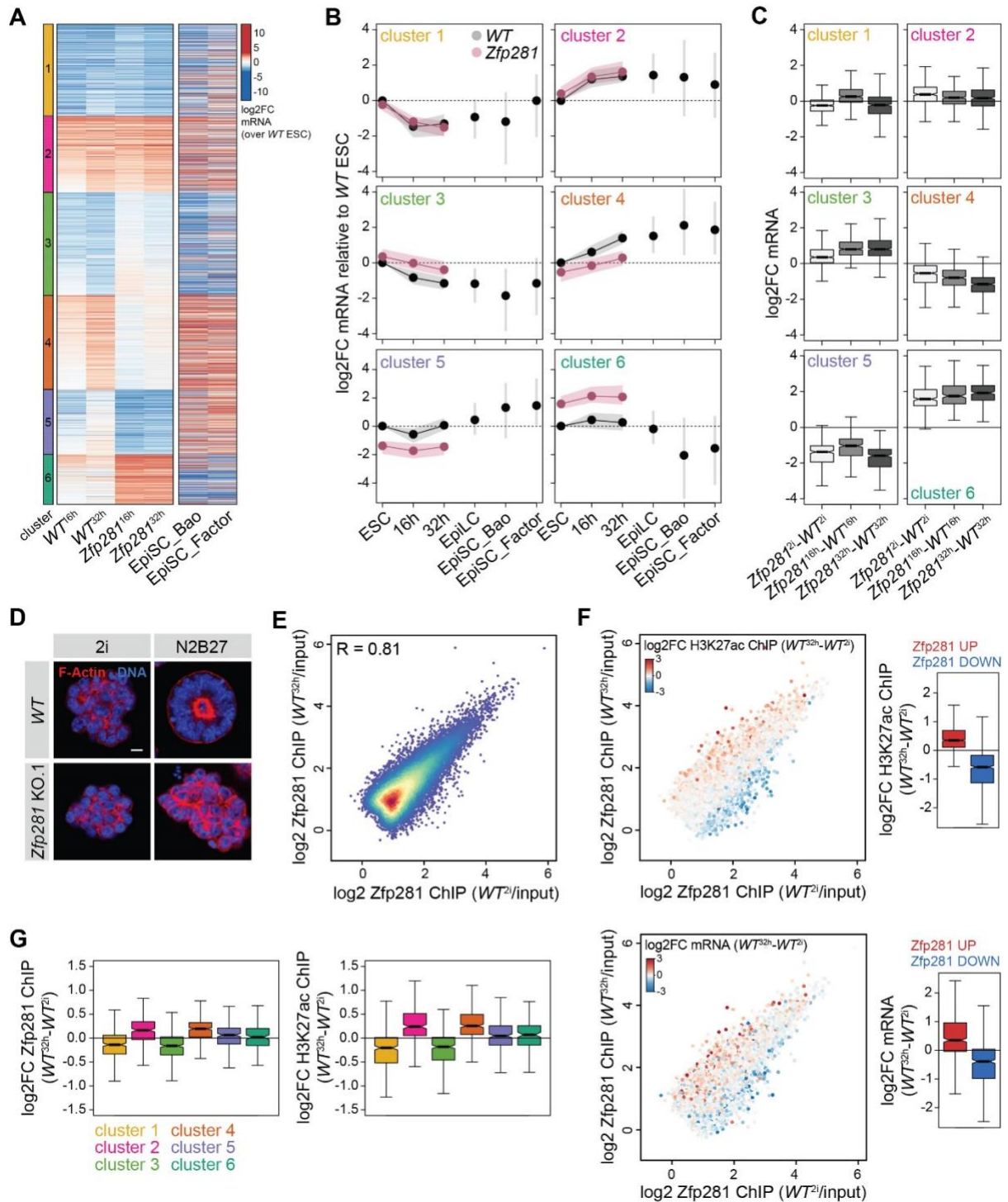


1 of undifferentiated (2i) and sorted GFP<sub>high,sort</sub> and GFP<sub>low,sort</sub> cells of indicated genotypes (bottom panel).  
2 Average and SD of 3 experiments performed in duplicates.

3 **(D)** Representative flow cytometry profiles of control and Zfp281-inducible ESCs (top panel) and  
4 quantification of GFP<sub>low</sub> cells (bottom panel) after 2d in 2i and in the presence (green) or absence (black)  
5 of Dox. Average and SD of 2 experiments.

6 **(F)** Zfp281 mRNA changes during ESC differentiation detected by quantitative PCR (left) and extracted  
7 from published RNA-seq datasets (Buecker *et al*, 2014; Factor *et al*, 2014; Boroviak *et al*, 2015; Bao *et*  
8 *al*, 2018) (right). Average and SD of 2 technical replicates (left).

Mayer et al., Figure 3



1

2 **Figure 3: Zfp281 directs sequential gene expression despite stable occupancy of target sites.**

3 (A) mRNA log<sub>2</sub> fold changes (log<sub>2</sub>FC) in *WT*<sub>16h</sub>, *WT*<sub>32h</sub>, *Zfp281*<sub>16h</sub> and *Zfp281*<sub>32h</sub> samples relative to  
 4 *WT*<sub>2i</sub> cells, and in EpiSCs relative to *WT*<sub>2i/Lif</sub> cells (Factor *et al.*, 2014; Bao *et al.*, 2018). *Zfp281*<sub>2i</sub>,  
 5 *Zfp281*<sub>16h</sub>, *Zfp281*<sub>32h</sub> and *WT*<sub>16h</sub> and *WT*<sub>32h</sub> samples were used for k-means clustering.

6 (B, C) Quantification of (A) including mRNA log<sub>2</sub>FC in EpiLCs relative to *WT*<sub>2i/Lif</sub> (Buecker *et al.*, 2014)  
 7 and as indicated (C).

- 1 **(D)** Representative immunofluorescence staining of spheroids in Matrigel derived from *WT* or *Zfp281*  
2 *KO.1* ESCs grown in 2i or N2B27 for 3d. Blue: DNA. Red: F-actin. Scale bar is 10 $\mu$ m.
- 3 **(E)** Scatter plot comparing *Zfp281* log<sub>2</sub> ChIP enrichment relative to matched inputs in *WT*<sub>2i</sub> and *WT*<sub>32h</sub>  
4 cells.
- 5 **(F)** Same as in **(E)** with dots colored according to H3K27ac ChIP log<sub>2</sub>FC at the same peaks (top left),  
6 and to gene expression log<sub>2</sub>FC associated with peaks by nearest distance to TSS (bottom left) in *WT*<sub>32h</sub>  
7 relative to *WT*<sub>2i</sub> cells. Quantification of H3K27ac ChIP (top right) and mRNA (bottom right) log<sub>2</sub>FC at  
8 top 1000 *Zfp281* peaks with increased (red) or decreased (blue) *Zfp281* binding during ESC  
9 differentiation.
- 10 **(G)** Quantification of *Zfp281* (left) and H3K27ac (right) ChIP log<sub>2</sub>FC in *WT*<sub>32h</sub> compared to *WT*<sub>2i</sub> cells at  
11 *Zfp281* peaks assigned to gene clusters 1-6.

## Mayer et al., Figure 4

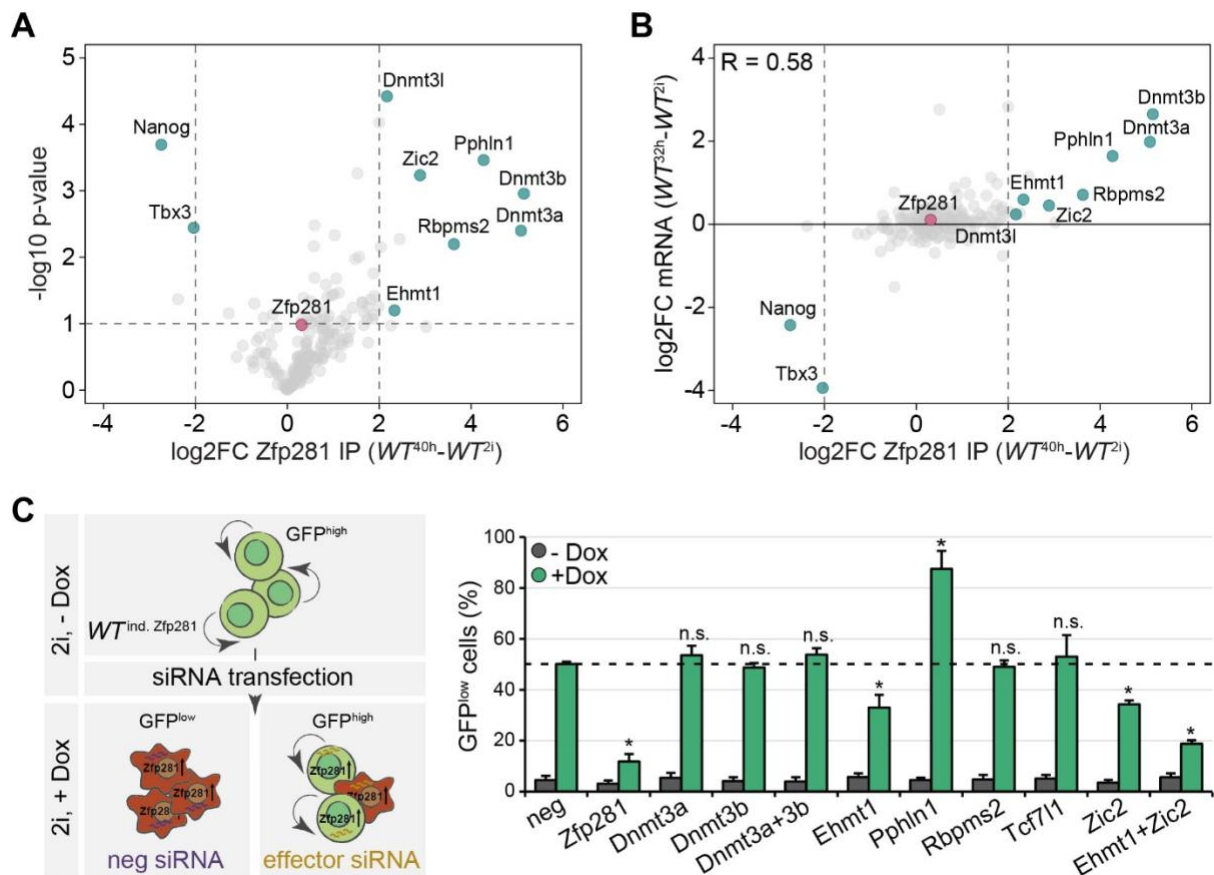


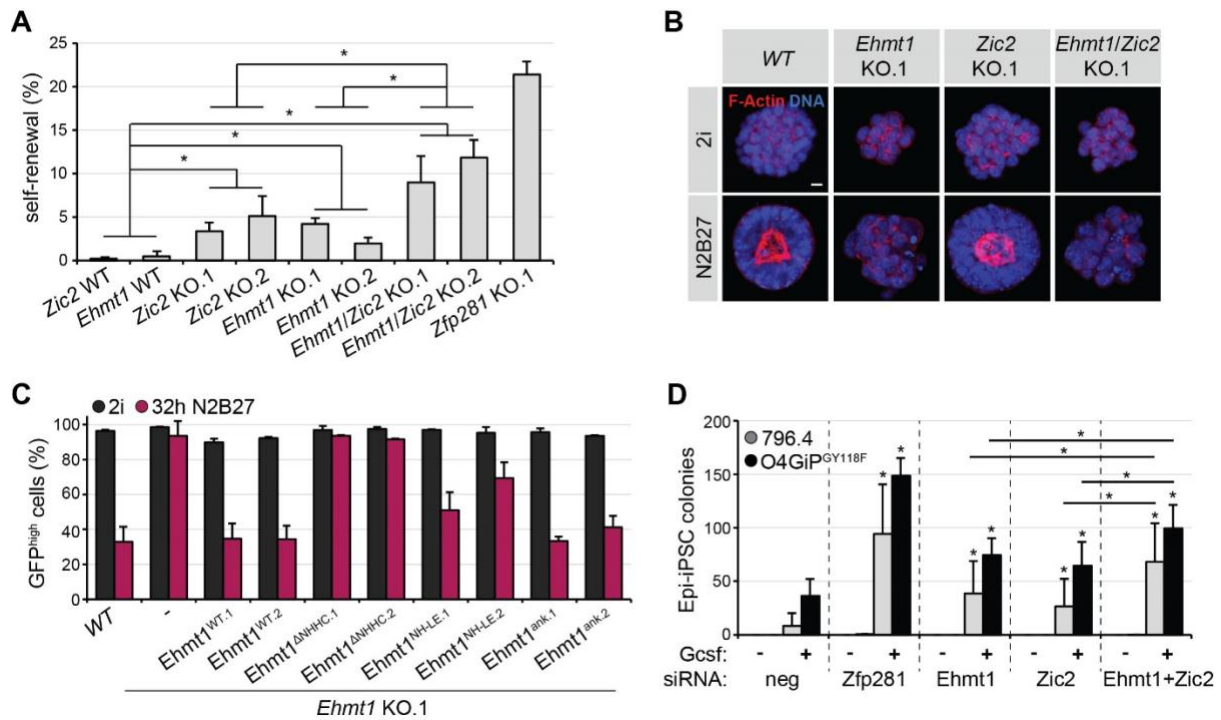
**Figure 4: Zfp281 acts by associating with Ehmt1 and Zic2.**

(A) Cell state-specific Zfp281 interactors in  $WT_{2i}$  and  $WT_{40h}$  cells. Pink and cyan mark Zfp281 and selected binding partners, respectively. Quantification is based on 3 biological replicates.

(B) Same as (A) with mRNA log2FC of differential binding partners during ESC differentiation instead of p-values.

(C) Procedure to identify Zfp281 effectors in naïve Zfp281-inducible RGd2 cells (left). Quantification of GFP<sup>low</sup>  $WT_{ind.}$  Zfp281 cells transfected with indicated siRNAs and incubated for 32h in 2i in the presence (green) or absence (black) of Dox (right). Dashed line marks fraction of GFP<sup>low</sup> cells in control cells exposed to Dox. Significance was determined using a Wilcoxon Mann-Whitney rank sum test compared to neg control sample. (\*) <math>p < 0.05</math>; not significant (n.s.). Average and SD of 4 experiments.

Mayer et al., Figure 5



1

2 **Figure 5: Ehmt1 and Zic2 drive exit from the ESC state and restrict reprogramming of EpiSCs.**

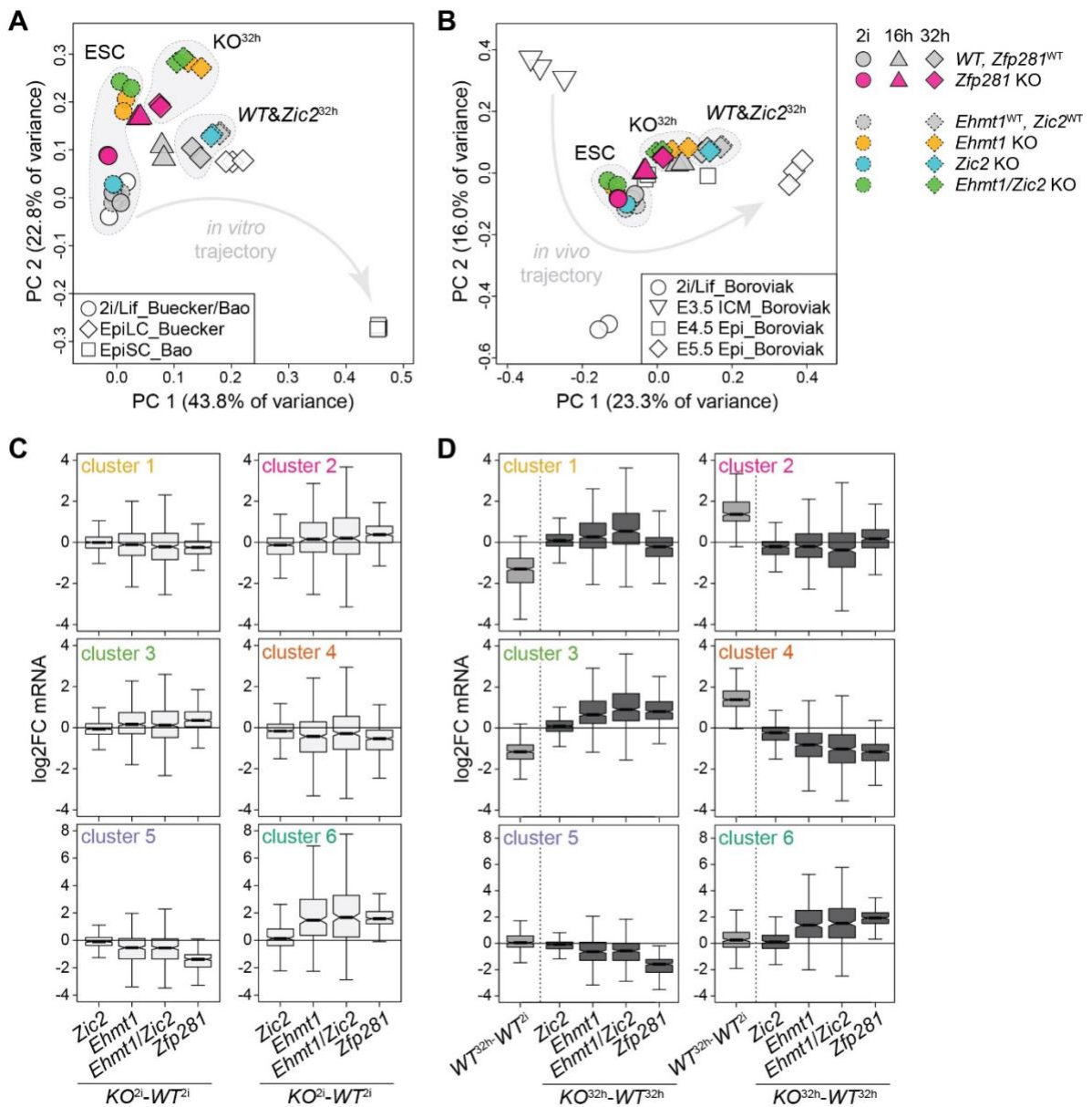
3 (A) Self-renewal in cells with indicated genotypes 3d after 2i withdrawal. Significance was determined  
 4 using a Wilcoxon Mann-Whitney rank sum test comparing the specified genotype groups. (\*) <0.05.  
 5 Average and SD of 2 experiments performed in duplicates.

6 (B) Representative immunofluorescence staining of spheroids in Matrigel derived from indicated  
 7 genotypes in 2i or N2B27 for 4d. Blue: DNA. Red: F-actin. Scale bar is 10µm.

8 (C) Quantification of GFP<sup>high</sup> cells in WT cells or Ehmt1 KO clones expressing indicated transgenes in  
 9 2i (black) or 32h after 2i withdrawal (pink). Average and SD of 2 experiments.

10 (D) Number of Epi-iPSC colonies derived from 796.4 (grey) and O4GIP<sup>GY118F</sup> (black) EpiSCs transfected  
 11 with indicated siRNAs, stimulated with Gcsf and 2i for 4d, and selected with Puromycin. Significance  
 12 was determined using a Wilcoxon Mann-Whitney rank sum test compared to neg control sample of the  
 13 respective cell line, or comparing Zic2 and Ehmt1 to Ehmt1/Zic2 depletion. (\*) <0.05. Average and SD  
 14 of 5 experiments performed in duplicates.

Mayer et al., Figure 6



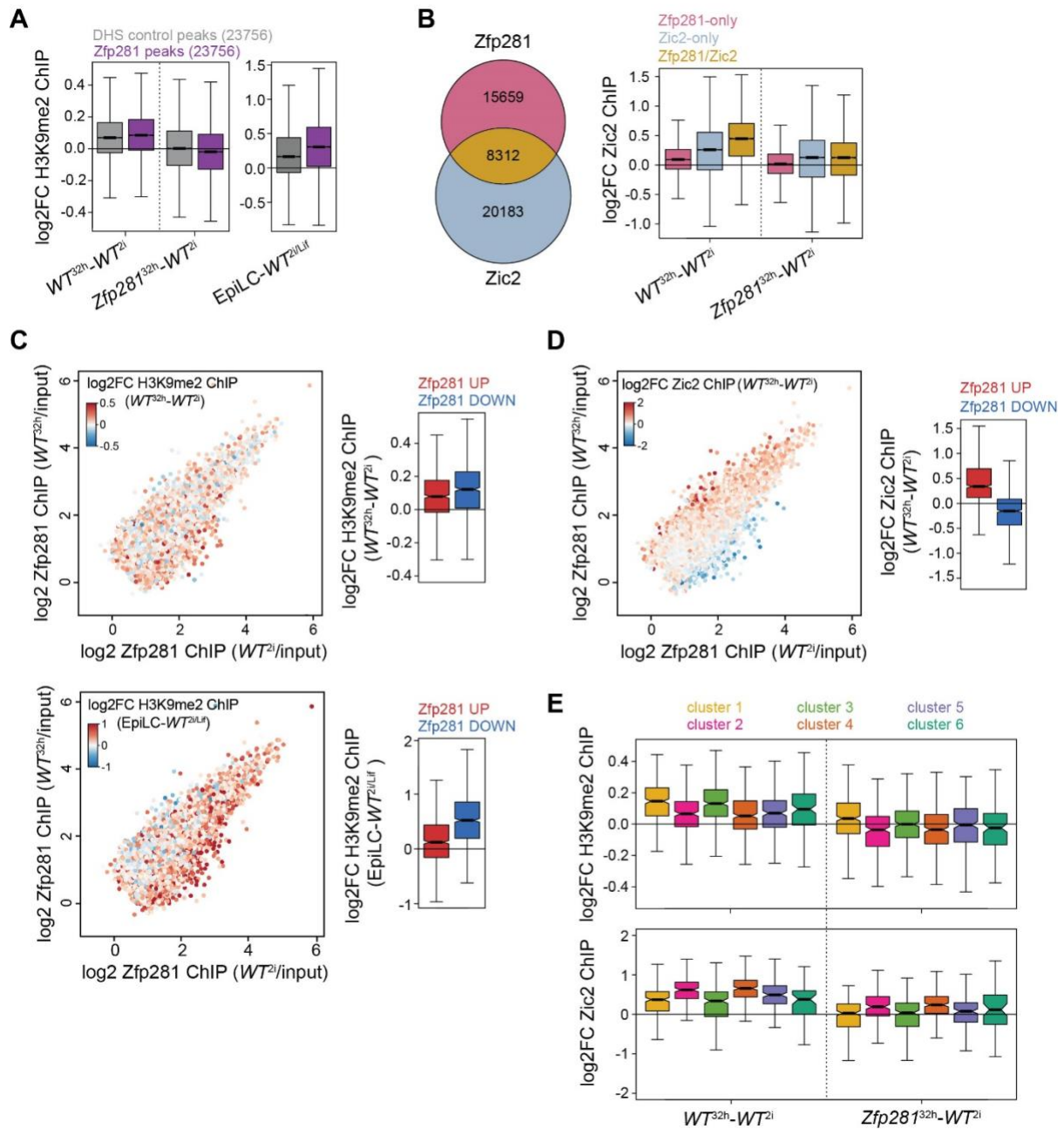
1

2 **Figure 6: Related transcriptional defects in *Ehmt1/Zic2* and *Zfp281* KO cells.**

3 (A, B) PC analysis of indicated samples normalized to WT ESCs (A) and all samples (B) within each  
4 dataset. Arrows indicate developmental trajectories. Full and dashed outlines indicate independent  
5 RNA-seq experiments.

6 (C, D) Quantification of cell state-specific mRNA log<sub>2</sub>FC of gene clusters 1-6 between indicated  
7 genotypes in 2i (C) and 32h after 2i withdrawal (D).

Mayer et al., Figure 7



1

2 **Figure 7: Zfp281 engages with Ehmt1 and Zic2 at developmental CREs.**

3 (A) H3K9me2 ChIP log<sub>2</sub>FC between indicated cell states and genotypes at 10kb windows surrounding  
4 Zfp281-bound (purple) or matching DNase-hypersensitive site (DHS) control peaks (grey).

5 (B) Overlap of Zfp281 and Zic2 ChIP peaks (left) and Zic2 ChIP log<sub>2</sub>FC between specified cell states  
6 and genotypes at indicated peak subsets (right).

7 (C, D) Same as in Figure 3F. Coloring is according to H3K9me2 ChIP log<sub>2</sub>FC between *WT*<sub>32h</sub> and *WT*<sub>2i</sub>  
8 cells (C, top left) and between EpiLCs and *WT*<sub>2i/Lif</sub> cells (C, bottom left) at Zfp281 peaks extended to  
9 10kb windows, and according to Zic2 ChIP log<sub>2</sub>FC between *WT*<sub>32h</sub> and *WT*<sub>2i</sub> cells (D, left).

- 1 Quantification of corresponding ChIP changes at top 1000 Zfp281 peaks with increased (red) or
- 2 decreased (blue) Zfp281 binding during ESC differentiation (right).
- 3 **(E)** H3K9me2 (top) and Zic2 (bottom) ChIP log<sub>2</sub>FC between indicated cell states and genotypes at all
- 4 Zfp281 peaks extended to 10kb windows (top) or Zfp281/Zic2 co-bound peaks (bottom) associated with
- 5 nearest TSSs of cluster 1-6 genes.



## 1 MATERIALS AND METHODS

### 2 Cell Culture

3 ESCs (male and female RGd2 cells containing a Rex1:GFPd2-IRES-Blasticidin (Wray *et al*, 2011), male  
4 O4GIP ESCs contain a GFP-IRES-Puromycin transgene under control of an Oct4 regulatory element  
5 (Betschinger *et al*, 2013) and male E14 cells) were cultured on plastic coated with gelatin or laminin  
6 (Sigma) in N2B27 medium (DMEM/F12 (Life Technologies), Neurobasal (Gibco) supplemented with N2  
7 (homemade) and B-27 Serum-Free Supplement (Gibco), 2mM L-glutamine (Gibco), and 0.1mM 2-  
8 mercaptoethanol (Sigma)) with 2i (3 $\mu$ M CHIR99021 and 1 $\mu$ M PD0325901 (Steward lab, Dresden)),  
9 and, where indicated, with 1 $\mu$ g/ml Doxycycline (Sigma). EpiSCs (O4GIP and OEC2 (Guo *et al*, 2009)  
10 and 796.4 (Yang *et al*, 2010)) were cultured on plastic coated with fibronectin (Millipore) in N2B27 with  
11 bFGF (12ng/ml) and ActivinA (20ng/ml) (FA) (Smith lab, Cambridge).

12 For monolayer differentiation, ESCs were seeded on gelatin-coated plates at  $1.5 \times 10^4$  cells/cm<sup>2</sup> in 2i  
13 and the following day 2i was withdrawn. Cells were incubated in N2B27 for 32 hours (h) or 72h, or  
14 continuously passaged on laminin-coated plates, as indicated. For EpiLC differentiation for 48h  
15 (Hayashi *et al*, 2011), medium was adjusted to FA and 1% knockout serum replacement (Thermo  
16 Fisher). For embryoid body (EB) differentiation, ESCs were seeded at  $2.5 \times 10^4$  cells/cm<sup>2</sup> on ultra-low  
17 attachment plates (Corning) in Serum media (GMEM (Sigma) supplemented with 10% fetal bovine  
18 serum (Sigma), 1mM sodium pyruvate (Gibco), 2mM L-glutamine (Gibco), 0.1mM non-essential amino  
19 acids (Gibco), and 0.1mM 2-mercaptoethanol (Sigma)) for 72h. Exit from pluripotency was quantified  
20 by measuring GFP fluorescence in RGd2 cells on a LSRII SORP Analyzer (Becton Dickinson) and  
21 analyzed using FlowJo (FlowJo, LLC), and by performing self-renewal and commitment assays as  
22 described before (Betschinger *et al.*, 2013). Briefly, differentiated RGd2 and E14 cells at indicated time  
23 points were plated at clonal density on laminin-coated plates in 2i medium, resulting colonies stained  
24 for alkaline phosphatase activity (Sigma) according to the manufacturer's instruction, and counted.  
25 RGd2 cells were additionally selected with 10 $\mu$ g/ml Blasticidin (Thermo Fisher). O4GIP cells were  
26 differentiated for 72h, treated with 2i medium containing 1 $\mu$ g/ml Puromycin (Gibco) and uncommitted  
27 cells quantified after 3 days by adding 1:10 diluted Alamar Blue (Invitrogen) in 2i medium, following by  
28 read out on a SpectraMax Gemini EM (Molecular Devices) microplate reader. For cell cycle analysis,  
29 cells were fixed in cold 70% ethanol for 30 minutes (min) at 4°C, washed twice with PBS and 0.1% BSA  
30 (Sigma), treated with 5 $\mu$ g RNaseA (Thermo Fisher) for 15min at room temperature (RT) and stained  
31 with 10 $\mu$ g propidium iodide (Sigma). Cells were analyzed on a LSRII SORP Analyzer and cell cycle  
32 distributions determined using FlowJo.

33 siRNA transfections were performed as described (Betschinger *et al*, 2013) using 16.7nM siRNA  
34 (detailed in Table **EV4**) and transfection mixes in OptiMEM (Invitrogen) containing Lipofectamine 2000  
35 or RNAiMAX (Thermo Fisher) for ESCs or EpiSCs, respectively.

36 For EpiSC reprogramming, cells were plated at  $1.5 \times 10^4$  cells/cm<sup>2</sup> on fibronectin-coated plates in N2B27  
37 with FA. The next day, medium was change to 2i and, as indicated, supplemented with 30ng/ml  
38 granulocyte colony stimulating factor (Gcsf) (Peprotech), 10ng/ml Lif (Smith lab, Cambridge) or 1 $\mu$ g/ml  
39 Doxycycline. After 4 days (d), medium was changed to 2i with 1 $\mu$ g/ml Puromycin, Epi-iPSC colonies

1 were stained for alkaline phosphatase activity, and counted. For experiments shown in Figure **1E** and  
2 **EV1A**, cells were subjected to self-renewal assays in 2i after 2 and 4d of Gcsf supplementation. For  
3 experiments shown in Figure **EV1E**, individual Epi-iPSC colonies were picked and expanded in 2i with  
4 Puromycin for further experiments.

5 Spheroid formation of ESCs was performed as described before (Shahbazi *et al*, 2017). Briefly, ESCs  
6 grown in 2i medium were washed in N2B27,  $7.5 \times 10^3$  cells were resuspended in 25 $\mu$ l ice-cold growth  
7 factor reduced Matrigel (Corning, 356231), plated dropwise on uncoated 96 well glass plates (Greiner  
8 Bio-One), and aggregated in N2B27 with or without 2i for 3 or 4d.

### 9 **EpiSC screen**

10 O4GIP<sub>GY118F</sub> EpiSCs were reverse-transfected in fibronectin-coated 384 well plates using mixtures of  
11 50ng esiRNA and 0.075 $\mu$ l Lipofectamine 2000 in 10 $\mu$ l OptiMEM medium. EpiSCs were plated at a  
12 density of 5000 cells/well in 80 $\mu$ l N2B27 with FA. Each plate included three negative (Luciferase  
13 esiRNA) and two positive (Stat3 esiRNA) control wells. The next day, medium was changed to 2i  
14 containing 30ng/ml Gcsf and 4d later to 2i containing 1 $\mu$ g/ml Puromycin. After 3-4d, medium was  
15 changed to 2i containing 1/10 vol Alamar Blue (Invitrogen) and cell survival quantified on a SpectraMax  
16 M2 (Molecular Devices).

### 17 **Genome editing**

18 CRISPR/Cas9 genome editing was performed by transient co-transfection of hCas9 and U6-gRNA  
19 plasmids (Mali *et al*, 2013) (Addgene plasmids 41815 and 41824) and a dsRed expression plasmid into  
20 E14 or female RGd2 ESCs. 2d later, single dsRed positive cells were sorted into gelatin-coated 96 well  
21 plates containing Serum media supplemented with 10ng/ml Lif and 2i. Clones were genotyped by  
22 sequencing amplified target loci, and by confirming protein absence in Western blots. For generation of  
23 knockout (KO) cell lines, two independent KO clones (specified in Figure **EV2A** and **J**, **EV4E** and **EV5A**)  
24 and, in the case of *Zfp281*, *Ehmt1* and *Zic2* targeting, one untargeted wildtype sibling clone were kept  
25 for further analysis.

26 N-terminal Flag-Avi tagging of *Ehmt1* was performed in *WT* or *Zfp281* KO ESCs constitutively  
27 expressing the BirA biotin ligase (see below). The recombination template was generated by cloning  
28 homology arms (548bp up- and 618bp downstream of the *Ehmt1* transcription start site) into  
29 pDONR221 using Gateway technology (Thermo Fisher) and inserting the Flag-Avi sequence by  
30 Seamless Cloning (Thermo Fisher). Targeting was performed as above with hCas9, U6-gRNA and  
31 dsRed expression plasmids, but included co-transfection of the recombination template, and genotyping  
32 the presence of biotinylated *Ehmt1* using Western blots.

33 gRNA sequences, genotyping primers and the *Ehmt1* recombination template are specified in Table  
34 **EV4**. gRNA sequences targeting *Tet1* and *Tet2* (Wang *et al*, 2013) and *Dnmt3a* and *Dnmt3b* (Domcke  
35 *et al*, 2015) have been described.

### 36 **Immunostaining**

1 Cells seeded on laminin-coated 96 well glass plates were fixed with 4% paraformaldehyde (Electron  
2 Microscopy Sciences) for 10min and spheroids grown in Matrigel for 20min at RT. Samples were  
3 blocked for 1h in blocking solution (PBS, 0.1% TritonX (Sigma), 3% donkey serum (Sigma), and 1%  
4 BSA) and incubated overnight with primary antibodies (Ehmt1 (Abcam, ab41969, 1:300) and H3K9me2  
5 (Abcam, ab12220, 1:300)) at 4°C. After three washes in washing solution (PBS, 0.1% TritonX),  
6 secondary antibodies were added, DNA stained with Hoechst33342 (Life Technologies) and, where  
7 indicated, incubated with Alexa Fluor 488 Phalloidin (Life Technologies, A12379, 1:40) for 20min at RT.  
8 Images were acquired using a LSM 710 scanning head confocal microscope (Zeiss) at 20x  
9 magnification and handled using Fiji and Adobe Photoshop (Adobe). Imaging of spheroids used for  
10 quantification in Figure **EV5G** was performed with a Yokogawa CV7000s high throughput confocal  
11 microscope at 20x magnification. Images were acquired in confocal mode as z-stack multiplane images  
12 over z distance of 50  $\mu\text{m}$  with a 5  $\mu\text{m}$  step size and maximum intensity projections were stored,  
13 representatives of which are shown in Figure **5B**.

#### 14 **Molecular biology**

15 Coding sequences for Ehmt1, Esrrb, Klf4 and Zfp281 were amplified from ESC complementary DNA  
16 (cDNA) and for BirA biotin ligase from a plasmid (gift of Matyas Flemr, Friedrich Miescher Institute,  
17 Basel). For Zic2, the coding sequence was synthesized as a double-stranded gBlock (IDT).  
18 Polynucleotides were recombined into pDONR221 using Gateway technology. Ehmt1 point mutations  
19 (Ehmt1 $\Delta$ NHHC: NHHC1198-1201del (Tachibana *et al*, 2008), Ehmt1<sup>NH-LE</sup>: NH1198-1199LE (Tachibana *et*  
20 *al*, 2008), and Ehmt1<sup>ank</sup>: W872A, W877A, E880A (Collins *et al*, 2008)) were introduced by polymerase  
21 chain reaction (PCR). Expression destination vectors were pPB-CAG-DEST-pgk-hph (Betschinger *et*  
22 *al*, 2013) and pPB-TRE-DEST-rTA-pgk-hph (Villegas *et al*, 2019), and GY118F expression vector as  
23 described (Yang *et al*, 2010). Stable integration into ESCs or EpiSCs after co-transfection with pBASE  
24 (Betschinger *et al*, 2013) was selected in the presence of 150 $\mu\text{g}/\text{ml}$  HygromycinB (Thermo Fisher).

25 For relative mRNA quantification, total RNA was isolated from indicated samples using RNeasy Mini  
26 Kit (Qiagen) and cDNA prepared using SuperScript III reverse transcriptase (Invitrogen). Quantitative  
27 PCR was performed using TaqMan Fast Universal PCR master mix (Applied Biosystems) with gene  
28 specific primers, either using the universal probe library (UPL, Roche) or Taqman system (Applied  
29 Biosystems), and a GAPDH probe (Applied Biosystems) for normalization. Oligonucleotide sequences  
30 and probes are listed in Table **EV4**.

#### 31 **Protein methods**

32 Cell lysates for Western blotting were generated in RIPA buffer (50mM Tris, pH 7.4, 150mM NaCl, 1mM  
33 EDTA, 1% Tx-100, and 0.1% SDS). Primary antibodies were anti-GAPDH (Sigma, G8795, 1:5000),  
34 anti-Ehmt1 (Abcam, ab41969, 1:500), anti-Tet1 (Millipore, 09-872, 1:1000), anti-Tet2 (Abcam,  
35 ab124297, 1:300), anti-Zic2 (Abcam, ab150404, 1:500), anti-Zfp281 (Bethyl Laboratories, A303-118A,  
36 1:500), and anti-Streptavidin coupled to HRP (Sigma, EV2438, 1:1000).

37 Nuclear immunoprecipitations (IPs) for Zfp281 were performed in three biological replicates using *WT*<sub>Zi</sub>,  
38 *Zfp281*<sub>Zi</sub>, *WT*<sub>40h</sub> and *Zfp281*<sub>40h</sub> cells. Cells were washed with cold PBS, resuspended in 5 packed cell

1 volume (pcv) of buffer A (10mM HEPES pH 7.9, 1.5mM MgCl<sub>2</sub>, and 10mM KCl), incubated for 10min  
2 on ice, and broke open using a Dounce homogenizer. Nuclei were pelleted at 3300g for 15min at 4°C,  
3 resuspended in 3 pcv of buffer B (20mM HEPES pH 7.9, 1.5mM MgCl<sub>2</sub>, 0.2mM EDTA, and 20%  
4 glycerol) supplemented with 420mM NaCl, Complete Mini protease, PhosSTOP phosphatase inhibitors  
5 (Roche) and 250U/ml Benzonase (Sigma), and incubated for 30min at 4°C on a rotating wheel.  
6 Insoluble material was pelleted at 25000g for 30min at 4°C, and the supernatant diluted with buffer B  
7 to a final concentration of 150mM NaCl and including 0.02% NP40. 1% of the supernatant was kept as  
8 input sample and the remainder incubated with 10µl Dynabeads ProteinG (Invitrogen) and 1µg Zfp281  
9 antibody (Bethyl Laboratories, A303-118A) for 1h at 4°C on a rotating wheel. Beads were collected on  
10 a magnetic rack for 2–3min to remove the supernatant, and washed 4 times in 1ml buffer B containing  
11 150mM NaCl and 0.02% NP40 for 10min each at 4 °C on a rotating wheel. For mass spectrometry,  
12 proteins were digested on the beads as described before (Villegas *et al*, 2019).

13 Whole cell lysate IPs using 1µg Zfp281 antibody (Bethyl Laboratories, A303-118A) were performed as  
14 described before (Villegas *et al*, 2019) using Dynabeads.

#### 15 **Chromatin immunoprecipitation (ChIP)**

16 For ChIP of endogenous proteins or histone modifications, 8 x 10<sup>6</sup> cells per IP were fixed for 10min with  
17 1.1% formaldehyde in fixing solution (0.1M NaCl, 1mM EDTA, 0.5mM EGTA, and 50mM HEPES pH  
18 7.5) at RT on a rotating wheel, and neutralized with glycine to a final concentration of 0.125M for 5min  
19 at RT. Cells were washed three times with ice cold PBS by spinning at 1600g for 5min at 4°C, incubated  
20 for 10min at 4°C on a rotating wheel with 1ml lysis buffer 1 (50mM HEPES pH 7.5, 140mM NaCl, 1mM  
21 EDTA, 10% glycerol, 0.5% NP-40, and 0.25% TritonX), pelleted, and incubated for a further 10min at  
22 4°C in 1ml lysis buffer 2 (10mM Tris pH 8.0, 200mM NaCl, 1mM EDTA, and 0.5mM EGTA). Nuclei were  
23 pelleted, resuspended in 140µl shearing buffer (50mM Tris pH 8.0, 10mM EDTA, and 1% SDS), and  
24 sonicated in Diagenode 15ml Falcon tubes for 25 cycles (30 seconds ON, 30 seconds OFF) in ice-cold  
25 water using a Bioruptor Plus (Diagenode). 10% of sonicated DNA was kept as input sample. Lysates  
26 were further pelleted at 14000g for 10min at 4°C and the supernatant diluted 1:10 with ChIP dilution  
27 buffer (50mM Tris pH 8.0, 167mM NaCl, 1.1% Tx-100, and 0.11% Na-Deoxycholate). Lysates were  
28 precleared over 10µl Dynabeads for 2h and incubated overnight at 4°C on a rotating wheel with the  
29 following antibodies: 2µg H3K27ac (Active Motif, 39135), 2µg H3K9me2 (Abcam, ab1220), 2µg Zic2  
30 (Abcam, ab150404), or 2µg Zfp281 (Bethyl Laboratories, A303-118A). The next day, 10µl Dynabeads  
31 were added and incubated with lysates for 1h at 4°C on a rotating wheel. Beads were washed with 1ml  
32 of the following buffers for 5min each at 4°C: twice with wash buffer 1 (50mM Tris pH 8.0, 0.1% SDS,  
33 0.1% Na-Deoxycholate, 1% TritonX, 150mM NaCl, 1mM EDTA, and 0.5mM EGTA), once with wash  
34 buffer 2 (50mM Tris pH 8.0, 0.1% SDS, 0.1% Na-Deoxycholate, 1% TritonX, 500mM NaCl, 1mM EDTA,  
35 and 0.5mM EGTA), once with wash buffer 3 (50mM Tris pH 8.0, 250mM LiCl, 0.5% Na-Deoxycholate,  
36 0.5% NP40, 1mM EDTA, and 0.5mM EGTA), and twice with wash buffer 4 (50mM Tris pH 8.0, 10mM  
37 EDTA, and 5mM EGTA). Finally, beads were eluted twice with 100µl elution buffer (0.1M NaHCO<sub>3</sub>, and  
38 1% SDS) for 15min at RT in a shaker at maximum speed, and combined supernatants de-crosslinked  
39 overnight by supplementation to 200mM NaCl and continuous shaking at maximum speed at 65°C. The

1 same procedure was followed for input samples by adjusting the total volume of elution buffer to 200µl  
2 and 200mM NaCl. The next day, DNA was purified using MinElute PCR Purification Kit (QIAGEN).

3 Bio-ChIP for Flag-Avi tagged Ehmt1 was performed as described before (Ostapcuk *et al*, 2018) with  
4 minor modifications. Briefly, 8 x 10<sup>6</sup> cells per IP were fixed for 8min with 1% formaldehyde in PBS at  
5 RT on a rotating wheel, and neutralized with adjusting glycine to a final concentration of 0.125M and  
6 incubation for 1min at RT and for 5min on ice. Cells were washed three times with ice cold PBS and  
7 pelleted at 1000g for 5min at 4°C. Cells were lysed in lysis buffers 1 and 2 as described above. Nuclei  
8 were washed once in 5ml NUC buffer (15mM HEPES pH 7.5, 60mM KCl, 15mM NaCl, and 0.32mM  
9 sucrose) and resuspended in 1ml NUC Buffer supplemented with Complete Mini protease inhibitors,  
10 3.3µl 1M CaCl<sub>2</sub>, and 2-3µl Micrococcal Nuclease (Cell Signaling, 10011S). Enzymatic activity was  
11 induced for 15min at 37°C and shaking at 1000rpm, and stopped by addition of 50µl of STOP solution  
12 (250mM EDTA, and 500mM EGTA) and 110µl of 10x ChIP buffer (167mM Tris pH 8.0, 1.67M NaCl,  
13 12mM EDTA, 10% TritonX, and 0.1% SDS) with a further incubation for 5min on ice. Nuclei were gently  
14 disrupted by sonication in Diagenode 15ml Falcon tubes for 8 cycles (5 seconds ON, 5 seconds OFF)  
15 in ice cold water using a Bioruptor Plus. Lysates were centrifuged at 14000g for 5min at 4°C, 5% of the  
16 supernatant was kept as input sample, and the remaining supernatant precleared for 2h over 10µl  
17 Dynabeads at 4°C on a rotating wheel. Chromatin was incubated for 1h with M-280 Streptavidin coupled  
18 Dynabeads (Invitrogen) at 4°C on a rotating wheel, and washed with 1ml of the following buffers for  
19 5min each at 4°C: twice with TE buffer (10mM Tris pH 8.0, and 1mM EDTA) supplemented with 2%  
20 SDS, once with high salt buffer (50mM HEPES pH 7.5, 500mM NaCl, 1mM EDTA, 1% TritonX, and  
21 0.1% Na-Deoxycholate), once with wash buffer 3 (see above) and twice with TE buffer. Beads were  
22 eluted in 60µl elution buffer (see above) supplemented with 2µl RNaseA (10mg/ml stock) and incubated  
23 for 30min at 37°C while mixing. After supplementation to 10mM EDTA, 10mM Tris pH 8.0 and 2µl  
24 ProteinaseK (10mg/ml, Promega), the beads suspension was further incubated for 3h at 55°C and  
25 overnight at 65°C while shaking. The same procedure was followed for input samples, including  
26 RNaseA and ProteinaseK digestion. DNA was purified using AMPure XP beads (Beckman Coulter).

## 27 **Sequencing libraries**

28 RNA from ESCs grown in 2i and 16h and 32h after 2i withdrawal was isolated using RNAeasy kit  
29 (Qiagen). For *Zfp281* KO and corresponding *WT* cells, total RNA was subjected to ribosomal RNA  
30 depletion using Ribozero removal kit (Illumina) followed by library construction using ScriptSeq V2  
31 library preparation kit (Illumina). For *Ehmt1*, *Zic2*, *Ehmt1/Zic2* KO and corresponding *WT* cells, RNA-  
32 seq libraries were prepared using TruSeq mRNA Library preparation kit (Illumina). ChIP-seq libraries  
33 were prepared using NEBNext Ultra kit (New England BioLabs) following the manufacturer's  
34 recommendations. Sequencing was performed on an Illumina HiSeq2500 machine (50bp single-end  
35 reads).

## 36 **Quantification and statistical analysis**

### 37 *Screen analysis*

1 For the EpiSC reprogramming screen Z scores were calculated for each plate, excluding the two outer  
2 most columns and rows (Table **EV1**). Screen replicates are presented in Figure **EV1B**. Average Z  
3 scores >2 were considered as screen hits, identifying 146 genes (Figure **1B**). We quantified their role  
4 in exit from the ESC state by extracting primary data for these 146 genes from two previous ESC  
5 differentiation studies (Betschinger *et al*, 2013; Li *et al*, 2018), and computing Z scores on this subset  
6 (Table **EV1**). 67 and 129 of the 146 genes were mapped on results from (Betschinger *et al*, 2013) and  
7 (Li *et al*, 2018), respectively, resulting in mapping of 130 genes in total. Average Z scores from both  
8 ESC differentiation screens are presented in Figure **1C**.

### 9 *Quantification of immunostaining*

10 Quantification of H3K9me2 was performed in CellProfiler3 (Broad Institute). Nuclei were identified using  
11 Hoechst33342 staining and average H3K9me2 and DNA fluorescence intensity per nucleus  
12 determined: *WT*<sub>2i</sub> (453 cells), *Zfp281*<sub>2i</sub> (574 cells), *WT*<sub>32h</sub> (465 cells), *Zfp281*<sub>32h</sub> (792 cells).

13 For quantification of d3 and d4 spheroids from two biological replicates, images were stitched to  
14 generate a single image per channel and per well, and used for object segmentation with Matlab  
15 (MathWorks). Segmented object outlines were exported and used for feature extraction with software  
16 package CellProfiler3. Extracted features (84 features) describing object area, shape and intensity were  
17 normalized within corresponding assay plates using Z score transformation and unified into a cross-  
18 comparable dataset. Normalized features were used to extract 10 principal components (PC), which  
19 were further used for unsupervised clustering with the software package PhenoGraph (Levine *et al*,  
20 2015). Unsupervised clustering returned 13 clusters, objects belonging to the 2 sparsest clusters were  
21 discarded as outliers based on extreme variance in measured features in the respective classes. To  
22 describe radial distribution of F-actin signal intensity, segmented objects were divided into 20 concentric  
23 regions of same width. Distribution of F-actin staining intensity was described as mean fraction of  
24 intensity per region (MeanFrac) whereby the total intensity in the given region was normalized to the  
25 fraction of object area corresponding to the region. Mean fractions of intensity per region were not Z  
26 scored as these values were normalized per object *ad initio*. Visualization in Figure **EV5G** shows the  
27 mean of F-actin signal in a given concentric ring of all d4 spheroids per genotype and medium condition:  
28 *WT*<sub>2i</sub> (559 spheroids), *Ehmt1*<sub>2i</sub> (349 spheroids), *Zic2*<sub>2i</sub> (292 spheroids), *Ehmt1/Zic2*<sub>2i</sub> (164 spheroids),  
29 *Zfp281*<sub>2i</sub> (324 spheroids), *WT*<sub>96h</sub> (437 spheroids), *Ehmt1*<sub>96h</sub> (228 spheroids), *Zic2*<sub>96h</sub> (202 spheroids),  
30 *Ehmt1/Zic2*<sub>96h</sub> (233 spheroids), *Zfp281*<sub>96h</sub> (547 spheroids). Heatmap was generated using a heatmap  
31 function from the Bioconductor package NMF (Gaujoux & Seoighe, 2010) (package version 0.21.0).

### 32 *Protein identification and quantification*

33 Relative quantification of mass-spec data from three biological replicates (Table **EV3**) was performed  
34 with MaxQuant (version 1.5.3.8) using Andromeda as search engine and label free quantification as  
35 described (Villegas *et al*, 2019). Briefly, the mouse subset of the UniProt version 2015\_01 combined  
36 with the contaminant DB from MaxQuant was searched and the protein and peptide FDR were set to  
37 0.01. For Figure **4A, B**, proteins were considered which passed an interaction threshold of an at least  
38 twofold enrichment in IPs from *WT*<sub>2i</sub> or *WT*<sub>40h</sub> lysates compared to matched *Zfp281* KO lysates with a  
39 significant p-value < 0.1, and were quantifiable with at least two unique razor peptides.

1 *RNA-seq and Gro-seq analysis*

2 RNA-seq reads from wildtype and mutant cells in 2i, and 16h and 32h after 2i withdrawal were aligned  
3 to the mouse GRCm38/mm10 genome using qAlign from the Bioconductor package QuasR (Gaidatzis  
4 *et al*, 2015) (package version 1.22.0) with default parameters except for `splicedAlignment=TRUE`.  
5 Published RNA-seq from ESCs cultured in 2i/Lif and EpiLC (Buecker *et al*, 2014) were 36bp reads, and  
6 therefore no spliced alignment could be performed. RNA-seq from ESCs cultured in 2i/Lif and EpiSCs  
7 (Factor *et al*, 2014; Bao *et al*, 2018), and global run-on sequencing (GRO-seq) data from 2i/Lif cultured  
8 ESCs (Dorigi *et al*, 2017) were 100bp and 50bp paired-end reads, respectively, and therefore  
9 `paired="fr"` was used. For *in vivo* embryo data (Boroviak *et al*, 2015), pre-existing alignments to mouse  
10 GRCm38/mm10 genome were downloaded from ArrayExpress (E-MTAB-2958) and used. Alignments  
11 were quantified for known UCSC genes obtained from the TxDb.Mmusculus.UCSC.mm10.knownGene  
12 package (package version 3.4.4) using qCount from the Bioconductor package QuasR with default  
13 parameters (Table **EV2**).

14 Only transcripts with at least 3 counts per million in at least two biological samples from this study were  
15 considered as expressed genes (total: 13,096 genes). For identification of significantly deregulated  
16 genes, edgeR (Robinson & Oshlack, 2010) (package version 3.24.0) was used and detected genes  
17 were fitted to two generalized linear models:

18 (a)  $\sim time + genotype + time:genotype$ : This model uses  $WT_{2i}$ ,  $WT_{16h}$ ,  $WT_{32h}$ ,  $Zfp281_{2i}$ ,  
19  $Zfp281_{16h}$  and  $Zfp281_{32h}$  expression datasets. Genes with a significant *time* coefficient are  
20 genes that change either between  $WT_{2i}$  and  $WT_{16h}$  or  $WT_{2i}$  and  $WT_{32h}$  cells, genes with a  
21 significant *genotype* coefficient are differentially expressed between  $Zfp281_{2i}$  and  $WT_{2i}$   
22 cells, and genes with a significant interaction term *time:genotype* are deregulated in  $Zfp281$   
23 KO cells specifically during 16h or 32h differentiation.

24 (b)  $\sim genotype$ : This model identifies genes that differ between  $Ehmt1_{2i}$  and  $WT_{2i}$  cells.

25 Raw P values were corrected for multiple testing by calculating false discovery rates (FDR). Significant  
26 genes were identified as genes with an absolute log<sub>2</sub> fold-change greater than 1.0 and an FDR of less  
27 than 0.01.

28 For visualization of RNA-seq data, except principal component analysis (PCA) in Figure **6A** and **6B** and  
29 heatmap of selected markers in Figure **EV6A**, log<sub>2</sub> fold-change values were used that were obtained  
30 from edgeR by fitting the indicated datasets to the following models:

31 (c)  $\sim time$  (EpiLCs or EpiSCs): EpiLCs (Buecker *et al*, 2014) or EpiSCs (Factor *et al*, 2014)  
32 compared to  $WT_{2i/Lif}$  (Buecker *et al*, 2014) and EpiSC compared to  $WT_{2i/Lif}$  (Bao *et al*, 2018)  
33 (used for Figure **3A, B**).

34 (d)  $\sim genotime$ :  $Zfp281_{16h}$  or  $Zfp281_{32h}$  compared to  $WT_{2i}$  (used for Figure **3A, B** and **EV3A**),  
35 where *genotime* is the combination of genotype and time.

36 (e)  $\sim genotype$  (cell state-specific): KO cells in 2i compared to  $WT_{2i}$ , or KO cells 16h or 32h  
37 after 2i withdrawal compared to  $WT_{16h}$  or  $WT_{32h}$ , respectively (used for Figure **3C** and **6C**,  
38 **D** and **EV6B-E**).

1 For heatmap visualization in Figure **3A** only significantly deregulated genes in at least one condition  
2 were considered (model (a): *time*, *genotype* or *time:genotype*; total: 2,495 genes) and the following log2  
3 contrast were used for clustering: *WT*<sub>16h</sub>-*WT*<sub>2i</sub>, *WT*<sub>32h</sub>-*WT*<sub>2i</sub>, *Zfp281*<sub>2i</sub>-*WT*<sub>2i</sub>, *Zfp281*<sub>16h</sub>-*WT*<sub>2i</sub>, *Zfp281*<sub>32h</sub>-  
4 *WT*<sub>2i</sub>, *Zfp281*<sub>16h</sub>-*WT*<sub>16h</sub> and *Zfp281*<sub>32h</sub>-*WT*<sub>32h</sub>. For heatmap visualization in Figure **EV6A**, RNA-seq read  
5 counts were normalized (divided by the total number of aligned reads (library size), multiplied with  
6 minimal library size, and added with a pseudocount of 8) and log2 transformed, and the mean of  
7 biological replicates was plotted. For visualization in Figure **EV6B**, significantly deregulated genes in  
8 *Ehmt1*<sub>2i</sub> (model (b): *genotype*) but not *Zfp281*<sub>2i</sub> (model (a): *genotype*) are highlighted. In Figure **3B**, dots  
9 represent the median and shades the lower and upper quartile of indicated samples. Boxplots were  
10 generated using the boxplot function in R with default parameters except outline=FALSE. Correlation  
11 plots (Figure **EV6C, D**) were generated using corrplot function from the Bioconductor package corrplot  
12 (<https://github.com/taiyun/corrplot>) (package version 0.84). Heatmaps (Figure **3A, EV3A** and **EV6A**)  
13 were generated using aheatmap function from the Bioconductor package NMF. For PCA represented  
14 in Figure **6A**, normalized (see above) and log2 transformed read counts were centered by subtracting  
15 the average of *WT* ESCs within each of the following four RNA-seq data sets: 1) *Zfp281* KO and  
16 corresponding *WT* samples from this study; 2) *Ehmt1*, *Zic2*, *Ehmt1/Zic2* KO and corresponding *WT*  
17 samples from this study; 3) *WT*<sub>2i/Lif</sub> cells and EpiLCs (Buecker *et al*, 2014); and 4) *WT*<sub>2i/Lif</sub> cells and  
18 EpiSCs (Bao *et al*, 2018). For PCA represented in Figure **6B**, normalized (see above) and log2  
19 transformed read counts were centered by subtracting the average over all samples within each of the  
20 following three RNA-seq data sets: 1) *Zfp281* KO and corresponding *WT* samples from this study; 2)  
21 *Ehmt1*, *Zic2*, *Ehmt1/Zic2* KO and corresponding *WT* samples from this study; 3) *WT*<sub>2i/Lif</sub> cells and  
22 embryo samples (Boroviak *et al*, 2015). Centered read counts for each PCA are provided in Table **EV2**  
23 and the detailed R code is provided in Appendix File **1**. PCA was performed using the prcomp function  
24 in R. Analyses of enriched gene sets (Figure **EV1C, EV3B** and **EV6B**) were performed using DAVID  
25 (Huang *et al*, 2009) (version 6.8) for GO terms of biological processes.

26 The linear model to estimate synergistic transcriptional effects of *Ehmt1* and *Zic2* (Figure **EV6E**) was  
27 fitted using lm function in R:

$$28 \quad \Delta Ehmt1/Zic2_i \sim \beta_E \Delta Ehmt1_i + \beta_Z \Delta Zic2_i + \beta_{int} \Delta Ehmt1_i : Zic2_i$$

29  $\Delta$ : transcriptional difference (KO – WT) of gene *i*

30  $\beta$ : regression coefficient:

31  $E$ : *Ehmt1*

32  $Z$ : *Zic2*

33  $int$ : non-additive interaction

#### 34 *ChIP-seq and DHS-seq analysis*

35 ChIP-seq data from this study, published datasets (Buecker *et al*, 2014; Huang *et al*, 2017; Ishiuchi *et*  
36 *al*, 2019) and DNaseI hypersensitive site sequencing (DHS-seq) (Encode; accession number:  
37 ENCSR000CMW) reads were aligned to mouse GRCm38/mm10 genome using qAlign from the  
38 Bioconductor package QuasR with default parameters. Published H3K4me3, H3K27me3 and  
39 H3K9me2 ChIP-seq data (Kurimoto *et al*, 2015) were aligned using Bowtie (Langmead *et al*, 2009)



1 (version 4.4.7) with parameter `-C` in colorspace. Alignments were sorted and indexed using SAMtools  
2 (package version 1.2), and all ChIP-seq data were quantified with qCount from the Bioconductor  
3 package QuasR. Read counts were normalized (divided by the total number of aligned reads (library  
4 size), multiplied with minimal library size and added with a pseudocount of 8) and log<sub>2</sub> transformed. For  
5 DHS-seq, reads per million (RPM) were calculated by dividing the total number of aligned reads,  
6 multiplying with one million, adding a pseudocount of 8 and log<sub>2</sub> transforming the data.

7 We observed a non-linear relationship in Zfp281 ChIP-seq data when comparing read counts in Zfp281  
8 peaks between ChIP-seq replicates in *WT*<sub>2i</sub>, and therefore performed loess regression using  
9 `normalizeBetweenArrays` function of the Bioconductor package `limma` (Ritchie *et al*, 2015) (package  
10 version 3.38.2) with `method=cyclingloess`.

11 In Ehmt1 ChIP-seq data we detected a variable dependency of read counts in genomic tiles on the tile's  
12 GC composition (GC bias) which was most pronounced in input samples. In order to reduce this bias,  
13 we used a loess-based normalization method: First, reads were counted in each sample in 10kb  
14 windows (either genome-tiling windows or windows centered on Zfp281 peaks and corresponding  
15 control windows, see below). The counts were then scaled (divided by the total number of aligned reads  
16 (library size)), multiplied with minimal library size, added with a pseudocount of 8, and log<sub>2</sub> transformed.  
17 A loess curve was fit to the log<sub>2</sub>-transformed counts as a function of the fraction of G+C bases in the  
18 window using the R function `loess` with `span = 0.3`. This fit robustly captures the global signal  
19 dependency on the underlying GC composition. GC-corrected log<sub>2</sub> read counts were then obtained by  
20 subtracting the values predicted by the loess fit from the observed log<sub>2</sub> read counts (residuals of the  
21 fit).

22 Zfp281 peaks were called on Zfp281 ChIP-seq reads in *WT*<sub>2i</sub> and *WT*<sub>32h</sub> cells using `Macs2` (Zhang *et*  
23 *al*, 2008) (version 2.1.1.20160309) with default parameters. Peaks that were at least 2-fold enriched (IP  
24 over respective inputs) in at least one of the four Zfp281 ChIP samples were considered (total: 23,756  
25 peaks) (Table **EV2**). For comparison of Zfp281 ChIP samples from this study to ChIP in EpiSCs (Huang  
26 *et al*, 2017) and TSCs (Ishiuchi *et al*, 2019), peaks were called on Zfp281 ChIP-seq reads in *WT*<sub>2i</sub>,  
27 *WT*<sub>32h</sub>, EpiSCs and TSCs. Peaks that were at least 2-fold enriched (IP over respective inputs) in at least  
28 one of the four Zfp281 ChIP samples from this study, in the one Zfp281 ChIP sample in EpiSCs or in  
29 one of the two Zfp281 ChIP samples in TSCs were considered (total: 27,435 peaks) and used for  
30 plotting (Figure **EV3E** and **F**). Zic2 peaks were called on Zic2 ChIP-seq reads in *WT*<sub>2i</sub>, *WT*<sub>32h</sub>, *Zfp281*<sub>2i</sub>  
31 and *Zfp281*<sub>32h</sub> cells. To quantitatively compare Zfp281 and Zic2 binding, both peak sets were combined  
32 and overlapping peak regions were merged using the function `reduce` from Bioconductor package  
33 `GenomicRanges` (Lawrence *et al*, 2013) (package version 1.34.0). Fused peaks were classified into  
34 single- or co-bound as follows: Peaks that were enriched at least 2-fold (IP over respective inputs) in at  
35 least one of the four Zfp281 ChIP samples and in at least one of the eight Zic2 ChIP samples were  
36 considered as co-bound (total: 8,312 peaks), while if detected only in Zfp281 ChIP or only in Zic2 ChIP  
37 samples were considered as Zfp281-only (total: 15,659 peaks) or Zic2-only (total: 20,183 peaks),  
38 respectively (Table **EV2**). Reads of H3K27ac ChIP-seq datasets were counted in Zfp281, Zic2 or  
39 Zfp281/Zic2 co-bound peaks and normalized as described above.

1 Zfp281 or Zfp281/Zic2 co-bound peaks were assigned to genes by calculating the distances of peak  
2 midpoint to the nearest transcriptional start site (TSS) using a set of non-redundant TSSs with a single  
3 start site randomly selected for each gene. Zfp281 peaks were classified as proximal if the distance to  
4 the nearest TSS was less than 2000bp (7,697 peaks) and as distal otherwise (16,059 peaks) (Figure  
5 **EV3G**). H3K27ac reads in *WT*<sub>2i</sub> and *WT*<sub>32h</sub> cells, and H3K4me1 (Buecker *et al*, 2014) and H3K4me3  
6 (Kurimoto *et al*, 2015) reads in *WT*<sub>2i/Lif</sub> and EpiLCs were counted in Zfp281 peak regions and normalized  
7 as described above. Proximal Zfp281 binding sites with at least 1.5-fold enrichment of H3K27ac over  
8 respective inputs in either *WT*<sub>2i</sub> or *WT*<sub>32h</sub> cells and with at least 2-fold enrichment of H3K4me3 over  
9 respective inputs in either *WT*<sub>2i/Lif</sub> cells or EpiLCs were considered as associated with active promoters  
10 (54% of proximal peaks, total: 4,128). Distal Zfp281 binding sites with at least 1.5-fold enrichment of  
11 H3K4me1 over respective inputs in either *WT*<sub>2i/Lif</sub> cells or EpiLCs were considered as putative  
12 enhancers (62% of distal peaks, total: 9,990), of which sites additionally enriched at least 1.5-fold over  
13 respective inputs in H3K27ac in either *WT*<sub>2i</sub> or *WT*<sub>32h</sub> cells were classified as active enhancers (38% of  
14 putative enhancers, total: 3,818). For quantification at target sites differentially bound by Zfp281 during  
15 differentiation (Figure **3F**, **7C**, **D**), the 1000 binding sites with strongest increase (Zfp281 UP) and  
16 decrease (Zfp281 DOWN) in Zfp281 ChIP signal in *WT*<sub>32h</sub> compared to *WT*<sub>2i</sub> were considered.

17 Due to the broad chromatin distribution of Ehmt1 and H3K9me2, ChIP-seq reads were first quantified  
18 in genome-tiling windows of 10kb which were generated using tileGenome function from Bioconductor  
19 package GenomicRanges with tilewidth=10000 and cut.last.tile.in.chrom=TRUE. In Figure **EV7C**, all  
20 10kb genome-tiling windows were separated in 5 bins with equal number of tiles but increasing Ehmt1  
21 ChIP log<sub>2</sub> enrichment over respective input in *WT*<sub>2i</sub> cells. To quantify Ehmt1 and H3K9me2 enrichment  
22 at Zfp281 binding sites, Zfp281 peak regions were extended to 10kb centered on the peak midpoint  
23 using the function resize from the Bioconductor package GenomicRanges. As a control set, DHS-seq  
24 peaks (peak annotation downloaded from ENCODE; accession number: ENCSR000CMW) were  
25 extended to 10kb centered on the peak midpoint and only regions non-overlapping with 10kb extended  
26 Zfp281 peaks were considered. The final set of control regions was obtained by randomly sampling one  
27 DHS 10kb peak per Zfp281 10kb peak, such that the distributions of DHS-seq signal (log<sub>2</sub> RPM) and  
28 GC-content between Zfp281 10kb extended peaks and the selected control regions matched closely.

29 Boxplots were generated using the boxplot function in R with default parameters except outline=FALSE.  
30 Genomic profiles for heatmaps centered on the Zfp281 peak midpoint (Figure **EV3G**) were generated  
31 with qProfile from the Bioconductor package QuasR, and visualized using ComplexHeatmap (package  
32 version 1.20.0) (Gu *et al*, 2016). Except for Zfp281 ChIP-seq and GRO-seq (Dorigi *et al*, 2017), the  
33 averages of two replicates are shown.

#### 34 **Details for quantification and statistical analysis in Figures**

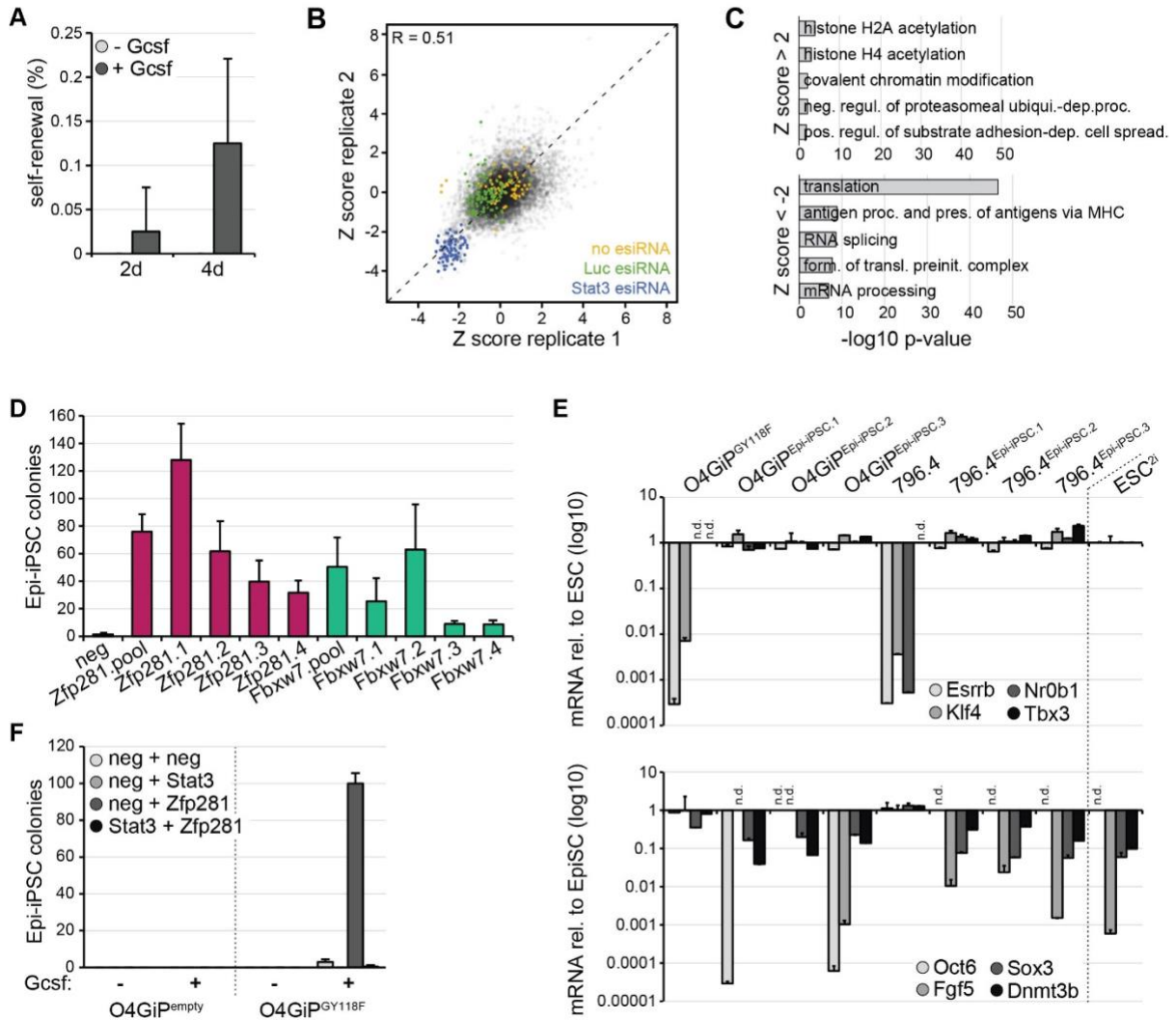
35 Details of experiments can be found in the figure legends, including number of biological or technical  
36 replicates and the statistical test used. All data quantification is represented as the mean and standard  
37 deviation (SD).

#### 38 **Data availability**

- 1 Next-generation sequencing data reported in this study have been deposited at the Gene Expression
- 2 Omnibus with accession number GSE131017. Reviewers can get access to the data by searching for
- 3 the above GSE identifier and then using the token kbsncwsufzknpgz.

1 EXTENDED VIEW FIGURES

Mayer et al., Figure EV1



2

3 **Figure EV1: Enhanced reprogramming of EpiSCs in the absence of Zfp281.**

4 (A) Self-renewal of O4GiP<sup>GY118F</sup> reprogramming intermediates after 2 or 4d in 2i in the presence or  
5 absence of Gcsf. Average and SD of 2 experiments performed in duplicates.

6 (B) Scatter plot of Z scores between screen replicates. Negative controls (no esiRNA and non-targeting  
7 Luc esiRNA) are marked in yellow and green, respectively, and positive controls (Stat3 esiRNA) in blue.  
8 Pearson's correlation coefficient (R).

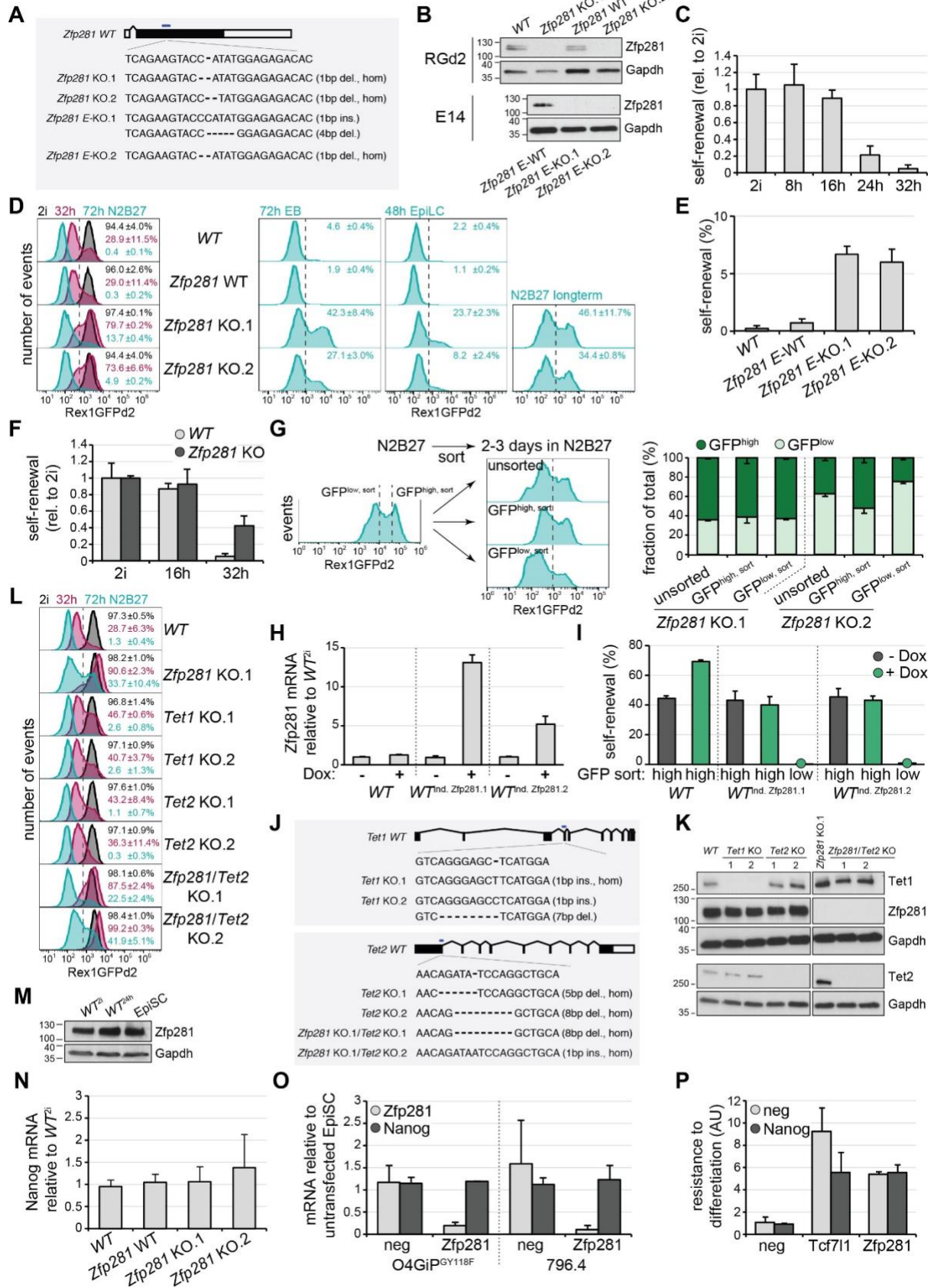
9 (C) Top 5 GO terms enriched in screen hits with Z scores > 2 (top) and < -2 (bottom).

10 (D) Deconvolution of siRNA pools: Epi-iPSC colonies derived from 796.4 EpiSCs transfected with  
11 indicated siRNAs (individual siRNAs or pools), stimulated for 4d with Gcsf and 2i, and selected with  
12 Puromycin. Average and SD of 3 experiments performed in duplicates.

13 (E) Induction of naïve (top) and repression of primed (bottom) pluripotency markers in Epi-iPSCs  
14 derived from Zfp281-depleted and Gcsf-stimulated O4GiP<sup>GY118F</sup> and 796.4 EpiSCs. mRNA fold changes

- 1 relative to ESCs (top) and EpiSCs (bottom) are shown on a log(10)-scaled axis. Average and SD of 2
- 2 technical replicates. Not detected (n.d.).
- 3 **(F)** Epi-iPSC colonies derived from O4GIP<sub>empty</sub> and O4GIP<sub>GY118F</sub> EpiSCs transfected with indicated
- 4 siRNAs, incubated for 4d in 2i in the presence or absence of Gcsf, and selected with Puromycin.
- 5 Average and SD of 2 technical replicates.

Mayer et al., Figure EV2



1 **Figure EV2: Characterization of Zfp281 and Tet enzymes in ESC differentiation.**

2 **(A, B)** Sequence of genome-edited *Zfp281* locus **(A)** and absence of protein **(B)** in KO cells. E denotes  
3 E14 parental cell line origin.

4 **(C, E, F)** Self-renewal in RGd2 cells **(C)** and of indicated genotypes **(E, F)** after 3d **(E)** or indicated  
5 timepoints **(C, F)** of 2i withdrawal. Average and SD of 2 experiments performed in duplicates.

6 **(D, L)** Representative flow cytometry profiles of RGd2 ESCs of specified genotypes, at indicated  
7 timepoints and in indicated conditions. Numbers are average and SD of GFP<sub>high</sub> cells in 2 experiments.

8 **(G)** Flow cytometry profiles (left panel) of longterm-differentiated *Zfp281* KO.2 cells in N2B27 and  
9 indicating GFP sorting gates (left), and of unsorted or sorted GFP<sub>low,sort</sub> and GFP<sub>high,sort</sub> cells after an  
10 additional 2-3 days of culture in N2B27 and indicating gates used for quantification of GFP distribution  
11 (right). Please note that profiles shown on the right were recorded on a different instrument than the  
12 profile presented on the left. Quantification of GFP distribution (right panel) in N2B27 cultures derived  
13 from indicated sorted cells of specified genotypes. Average and SD of 2 experiments.

14 **(H)** *Zfp281* transcription relative to untreated *WT*<sub>2i</sub> cells in *Zfp281*-inducible ESC clones after 48h in 2i  
15 and in the presence or absence of Dox. Average and SD of 2 technical replicates.

16 **(I)** Self-renewal of sorted GFP<sub>high,sort</sub> and GFP<sub>low,sort</sub> populations of indicated genotypes after exposure  
17 to Dox (green) or control conditions (black) for 48h. Green circles on x axis mark Dox-treated non-self-  
18 renewing samples. Average and SD of 2 technical replicates.

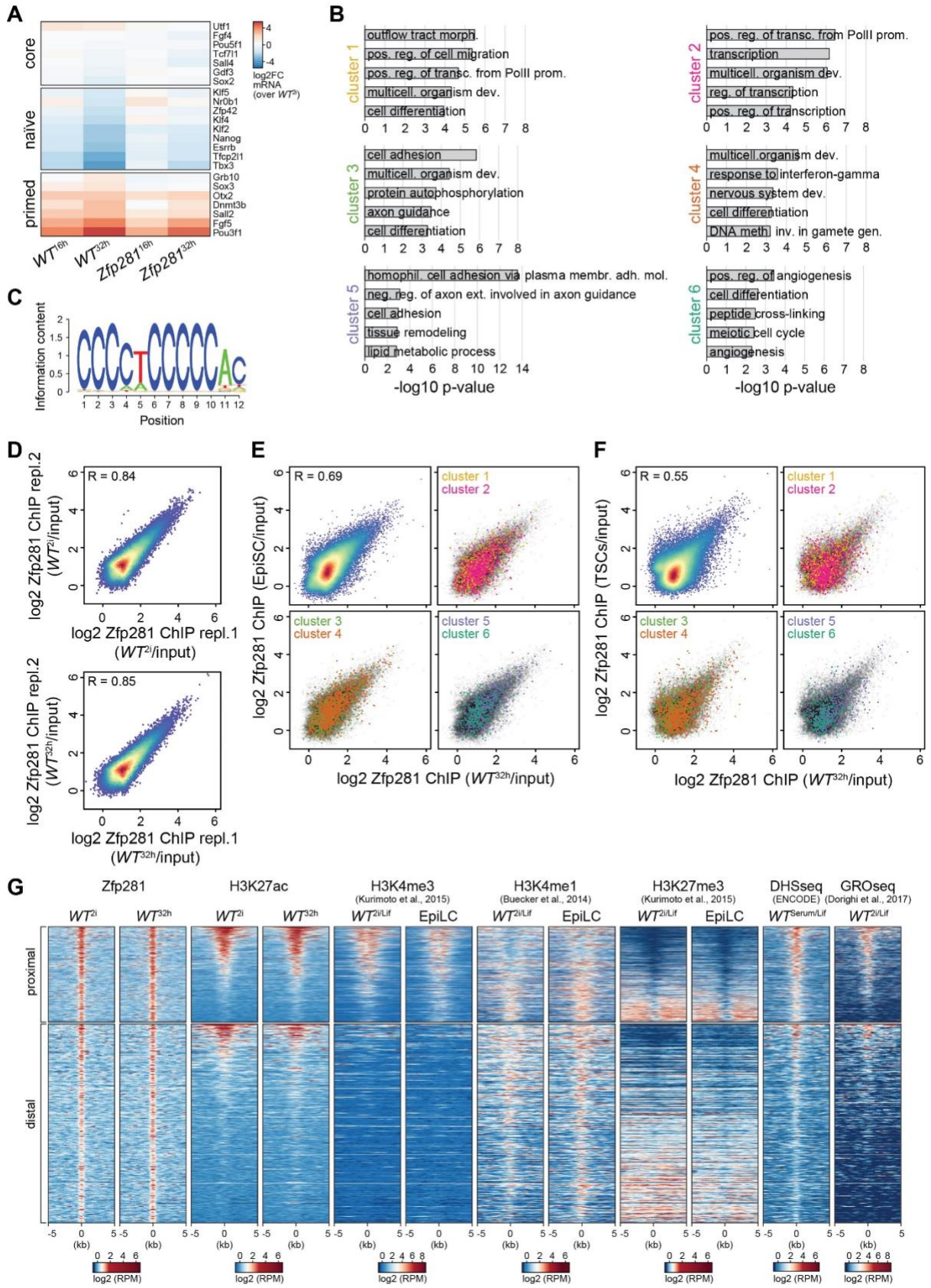
19 **(J, K)** Sequence of genome-edited *Tet1* and *Tet2* loci **(J)** and absence of proteins **(K)** in KO cells.

20 **(M)** Western blot showing *Zfp281* protein levels during ESC progression.

21 **(N,O)** Nanog **(N,O)** and *Zfp281* **(O)** mRNA levels relative to *WT*<sub>2i</sub> cells in ESCs of specified genotypes  
22 **(N)** and in indicated EpiSCs 24h after transfection of neg and *Zfp281* siRNAs **(O)**. Average and SD of  
23 5 **(N)** and 2 **(O)** experiments performed in duplicates.

24 **(P)** Resistance to differentiation in O4GIP ESCs transfected with indicated siRNA combinations after  
25 3d of 2i withdrawal relative to untransfected cells. Average and SD of 2 experiments performed in  
26 duplicates.

Mayer et al., Figure EV3





1 **Figure EV3: Genomics of Zfp281.**

2 (A) mRNA log<sub>2</sub>FC relative to *WT*<sub>2i</sub> cells of selected core, naïve and primed pluripotency markers in  
3 differentiating *WT* and *Zfp281* KO cells at indicated timepoints.

4 (B) Top 5 enriched GO terms in clusters 1-6.

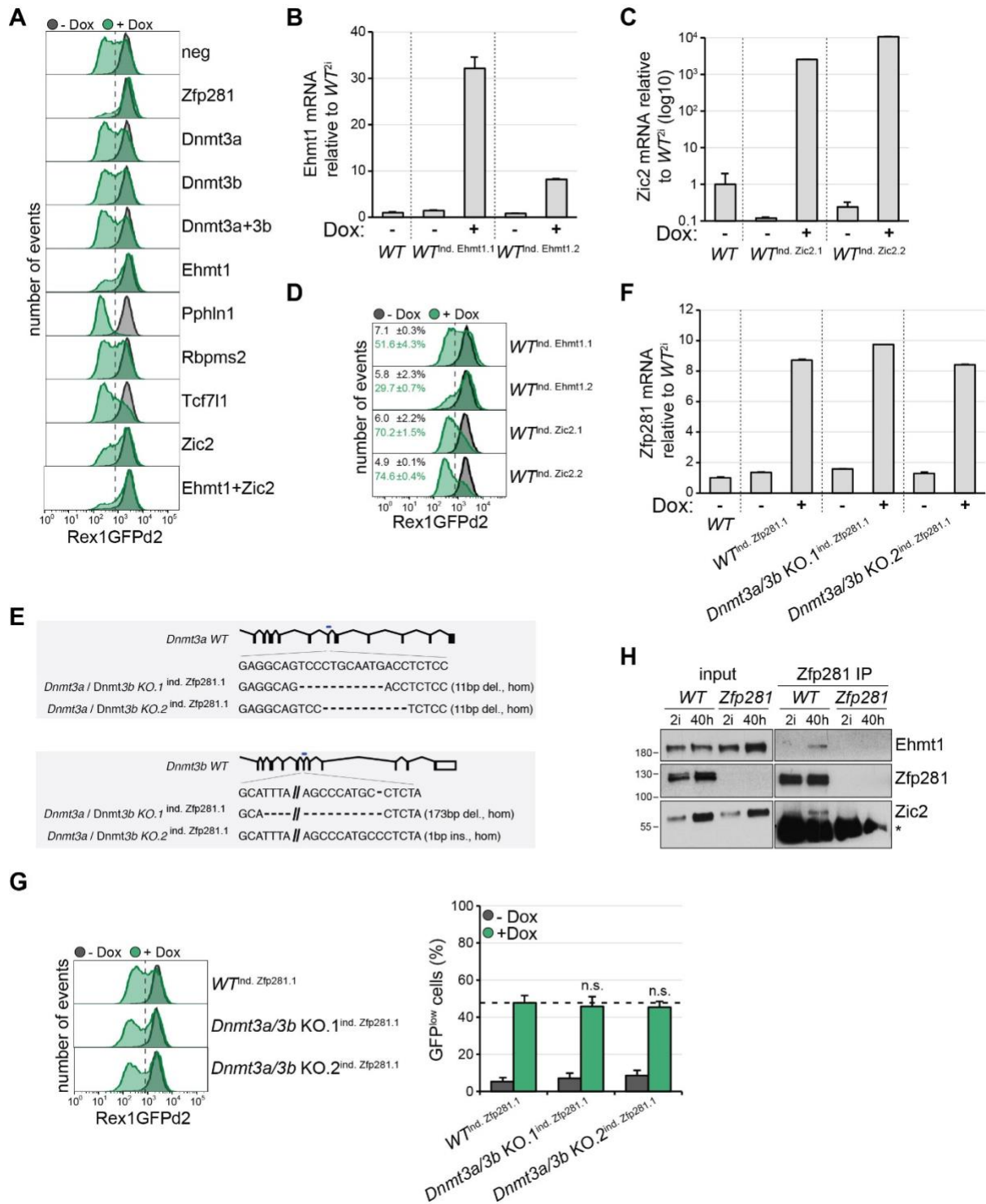
5 (C) Sequence logo from the *de novo* identified binding motif in 82.4% of 23756 *Zfp281* peaks.

6 (D) Scatter plot comparing log<sub>2</sub> *Zfp281* peak ChIP enrichment over matched inputs between replicates  
7 in *WT*<sub>2i</sub> (top) and *WT*<sub>32h</sub> (bottom) cells.

8 (E, F) Scatter plot comparing log<sub>2</sub> *Zfp281* ChIP enrichment over matched inputs in *WT*<sub>32h</sub> cells and  
9 EpiSCs (Huang *et al*, 2017) (E) and TSCs (Ishiuchi *et al*, 2019) (F). Peaks were assigned to closest  
10 transcriptional start sites (TSSs) and colored according to association with gene clusters 1-6.

11 (G) Heatmap of *Zfp281*, H3K27ac, histone H3 K4 tri-methylation (H3K4me<sub>3</sub>), H3K4 mono-methylation  
12 (H3K4me<sub>1</sub>) and histone H3K27 tri-methylation (H3K27me<sub>3</sub>) ChIPseq, DNase-hypersensitive sites  
13 (DHS) and global run-on sequencing (GROseq) read densities across all proximal (+/- 2kb of TSS)  
14 *Zfp281* (top) and distal *Zfp281* (bottom) peaks. Each row represents a 10kb window centered on the  
15 peak mid of *Zfp281*. Rows are sorted for H3K27ac ChIP read densities in ESCs. Reads per million  
16 (RPM).

Mayer et al., Figure EV4



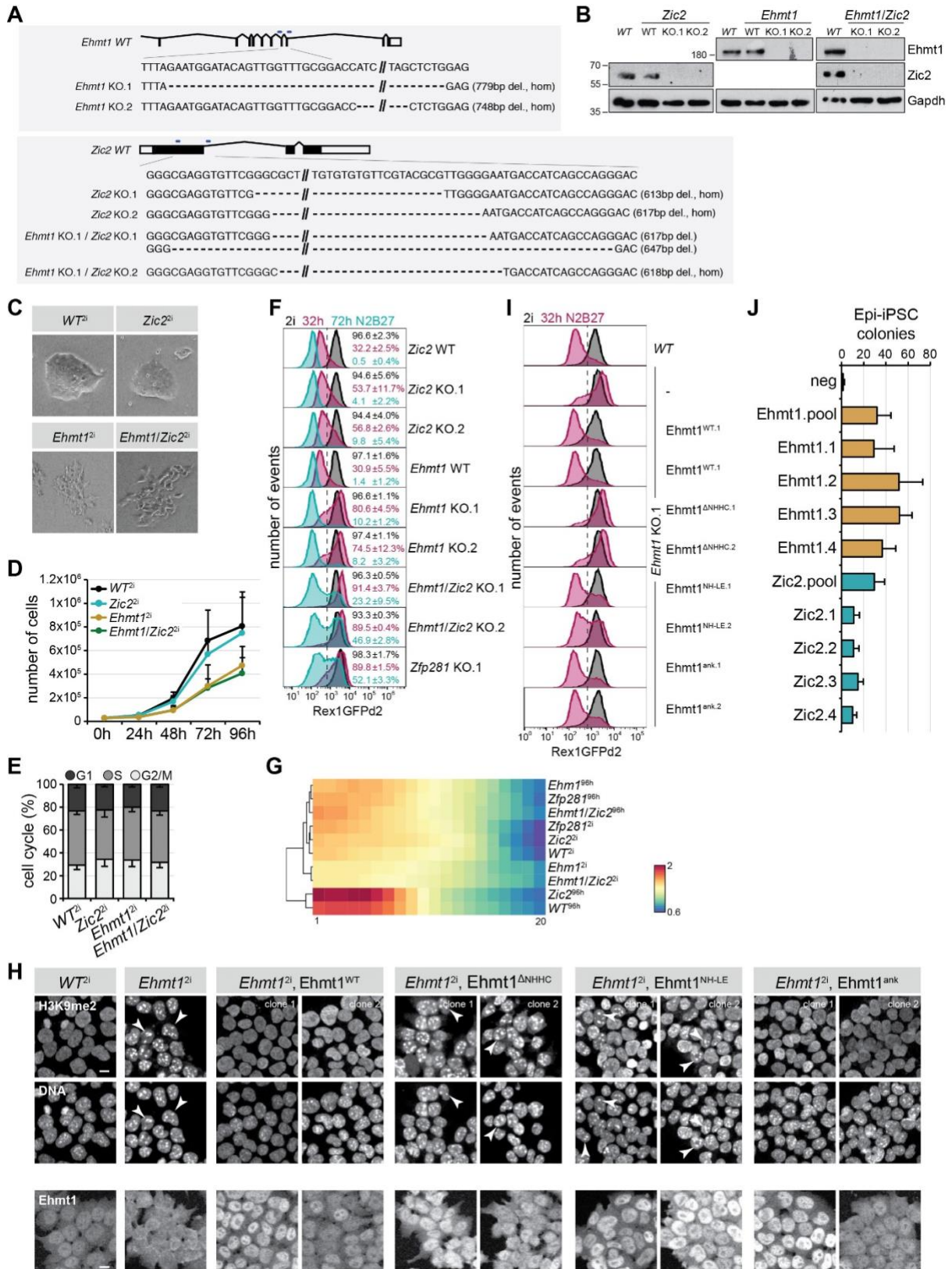
1

2 **Figure EV4: Characterization of Ehmt1 and Zic2 downstream of Zfp281.**

3 (A, D, G) Representative flow cytometry profiles of Zfp281-inducible RGd2 ESCs transfected with  
 4 indicated siRNAs (A), of RGd2 ESCs with conditional Ehmt1 and Zic2 expression (D), and of *Dnmt3a/3b*  
 5 compound KO RGd2 ESCs with conditional Zfp281 expression (G) after 32h in 2i and in the presence  
 6 (green) or absence (black) of Dox. Significance (G) was determined using a Wilcoxon Mann-Whitney

- 1 rank sum test compared to *WT*<sub>ind. Zfp281.1</sub> Dox-treated cells. not significant (n.s.) $\geq 0.05$ . Numbers are the
- 2 average and SD of GFP<sub>low</sub> cells in 2 (**D**) and 4 (**G**) experiments.
- 3 (**B, C, F**) FC Ehmt1 (**B**), Zic2 (**C**) and Zfp281 (**F**) transcription relative to untreated *WT*<sub>2i</sub> cells in indicated
- 4 ESC clones after 32h in 2i in the presence or absence of Dox. Average and SD of 2 technical replicates.
- 5 (**E**) Sequences of genome-edited *Dnmt3a* and *Dnmt3b* loci in *WT*<sub>ind. Zfp281.1</sub> cells.
- 6 (**H**) Whole cell lysate Zfp281 IPs in *WT* and *Zfp281* KO cells in 2i or 40h after 2i withdrawal, and probed
- 7 for indicated proteins. Input (left) and Zfp281 IP (right). (\*) Ig heavy chain.

Mayer et al., Figure EV5



1 **Figure EV5: Characterization of *Ehmt1*, *Zic2* and *Ehmt1/Zic2* KO cells.**

2 **(A, B)** Sequence of genome-edited *Ehmt1* and *Zic2* loci **(A)** and absence of proteins **(B)** in KO cells.

3 **(C-E)** Cell morphologies **(C)**, growth curves **(D)** and cell cycle analyses using propidium iodide staining  
4 **(E)** of indicated genotypes in 2i. Average and SD of 3 experiments **(D, E)**.

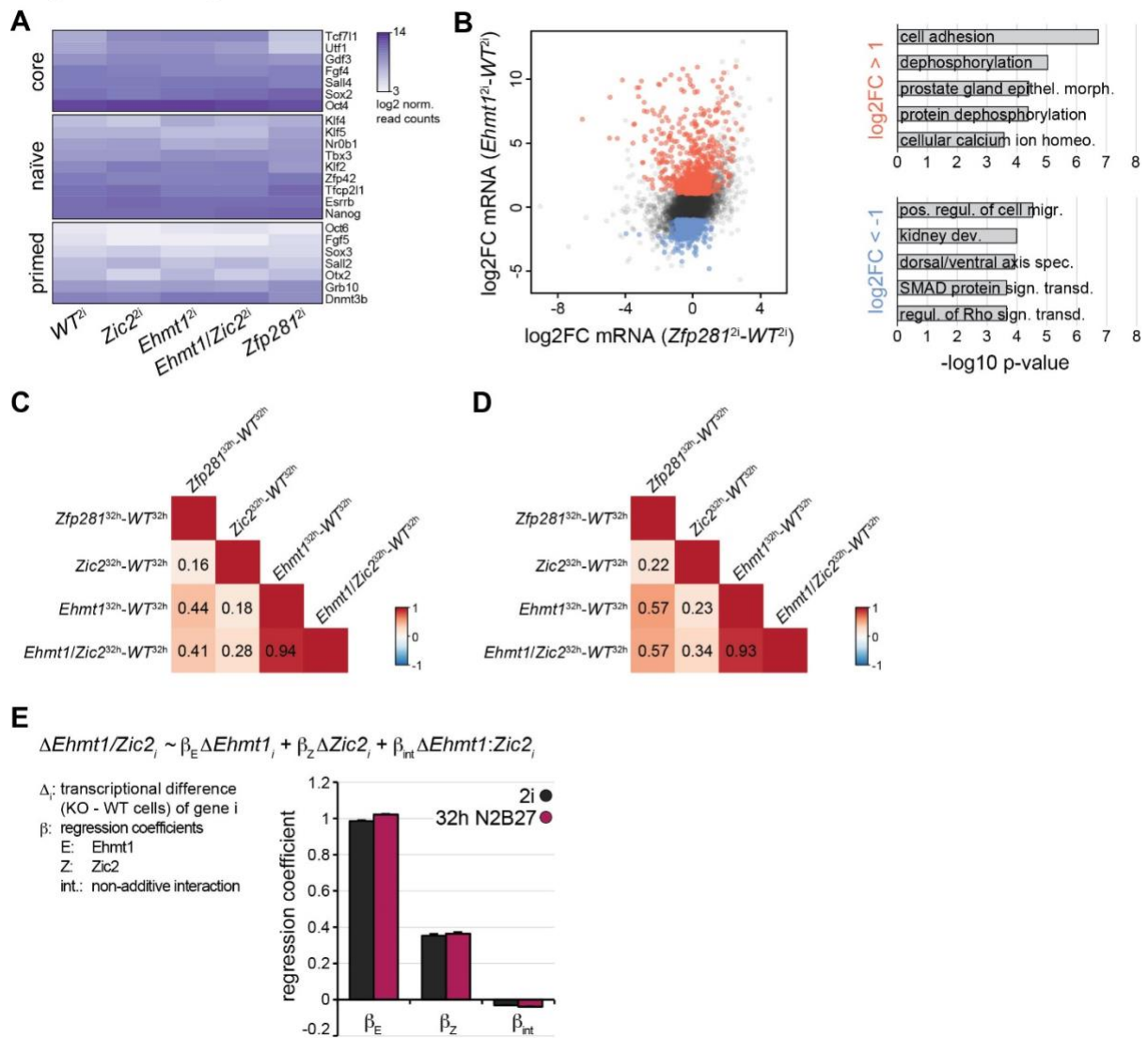
5 **(F, I)** Representative flow cytometry profiles of indicated genotypes in 2i, and after 32h and 72h of 2i  
6 withdrawal **(F)**, and in 2i and 32h after 2i withdrawal **(I)**. Numbers **(F)** are the average and SD of GFP<sup>high</sup>  
7 cells in 2 experiments.

8 **(G)** Quantification and hierarchical clustering of normalized F-actin intensity in 20 concentric rings (from  
9 center to circumference) in spheroids derived from ESCs with indicated genotypes in 2i or N2B27 for  
10 4d. Intensity is color-coded and illustrates central F-actin accumulation and, hence, polarization of *WT*  
11 and *Zic2* KO cells during differentiation.

12 **(H)** Representative immunofluorescence staining of *WT* or *Ehmt1* KO ESCs expressing the indicated  
13 transgenes. Top: H3K9me2 and DAPI. Bottom: Ehmt1. Co-localization of H3K9me2 with DAPI-rich  
14 speckles in *Ehmt1*<sub>2i</sub> cells expressing no transgene, the ΔNHHC, or NH-LE alleles is indicated by  
15 arrowheads. Please note absence of nuclear Ehmt1 staining in *Ehmt1*<sub>2i</sub> cells and restoration by Ehmt1  
16 transgenes. Scale bar is 10μm.

17 **(J)** Deconvolution of siRNA pools: Epi-iPSC colonies derived from 796.4 EpiSCs transfected with  
18 indicated siRNAs (individual siRNAs or pools), stimulated for 4d with Gcsf and 2i, and selected with  
19 Puromycin. Average and SD of 3 experiments performed in duplicates.

## Mayer et al., Figure EV6



1

### 2 **Figure EV6: Ehmt1 and Zic2 transcriptomics.**

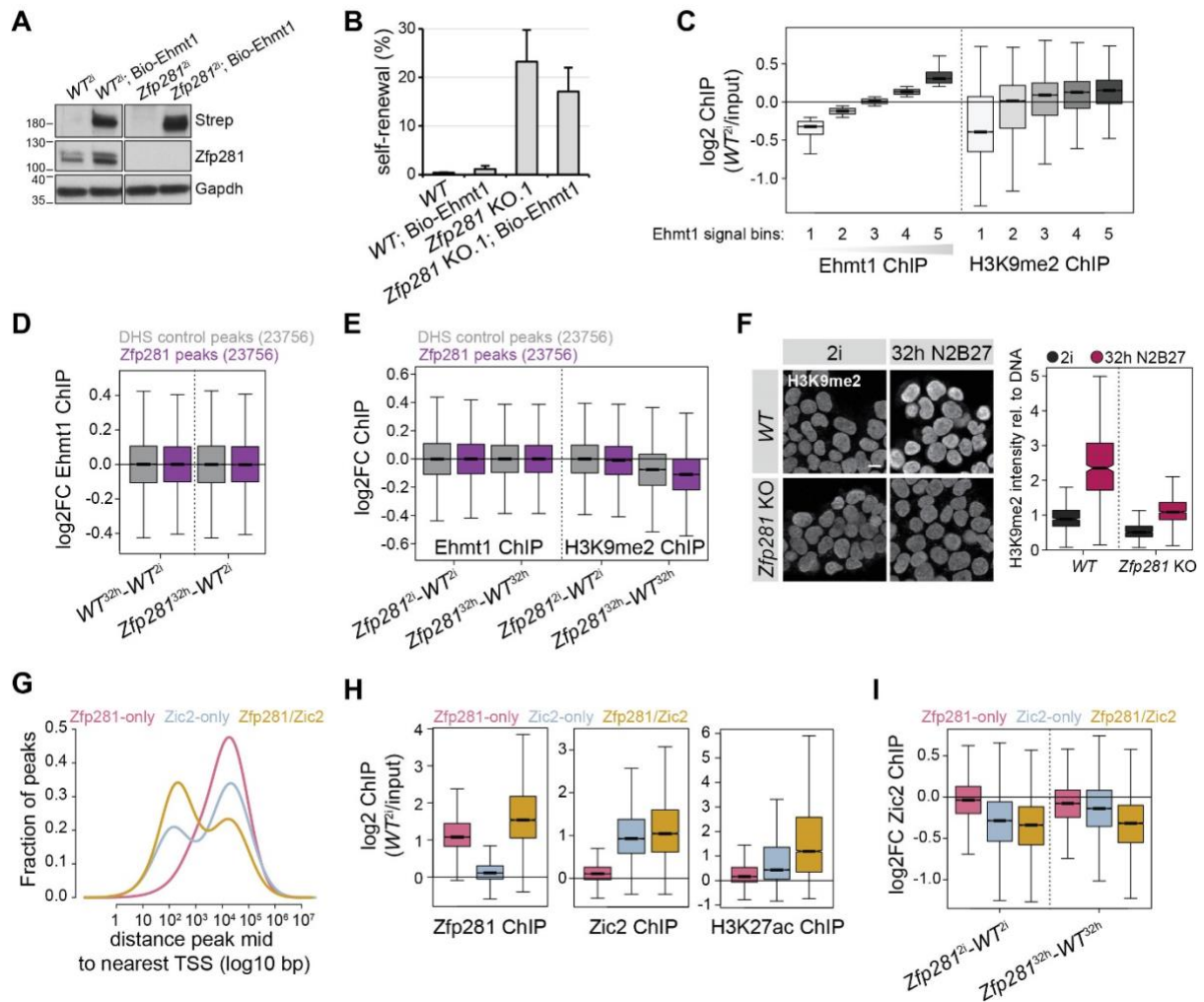
3 (A) log<sub>2</sub> normalized read counts of selected core, naïve and primed pluripotency markers in ESCs of  
 4 indicated genotypes.

5 (B) Scatter plot of mRNA log<sub>2</sub>FC in *Zfp281*<sup>2i</sup> and *Ehmt1*<sup>2i</sup> cells (left). Top 5 GO terms enriched in genes  
 6 upregulated (red) and downregulated (blue) specifically in *Ehmt1*<sup>2i</sup> cells (right).

7 (C, D) Pairwise Pearson correlation coefficients of mRNA changes between indicated differentiated  
 8 cells considering all detected transcripts (C) or gene cluster 1-6 transcripts (D).

9 (E) Estimated regression coefficients for the contribution of *Ehmt1* ( $\Delta Ehmt1$ ), *Zic2* ( $\Delta Zic2$ ) and their  
 10 interaction ( $\Delta Ehmt1:Zic2$ ) to cell state-specific gene expression changes in *Ehmt1/Zic2* compound KO  
 11 cells.

Mayer et al., Figure EV7



1

2 **Figure EV7: DNA binding of Ehmt1 and Zic2.**

3 (A) Western blot confirming Ehmt1 biotinylation (probed with Streptavidin (Strep)) in ESCs of indicated  
4 genotypes expressing the BirA ligase.

5 (B) ESC self-renewal of indicated genotypes after 3d of 2i withdrawal. Average and SD of 3 experiments  
6 performed in duplicates.

7 (C) Log2 Ehmt1 and H3K9me2 ChIP enrichment in ESCs over matched inputs at five classes of 10kb  
8 genome-wide windows binned by increasing Ehmt1 chromatin association.

9 (D, E) Ehmt1 (D, E) and H3K9me2 (E) ChIP log2FC between indicated cell states and genotypes at  
10 Zfp281 peaks (purple) or matching and non-overlapping DHS control peaks (grey) extended to 10kb  
11 windows.

12 (F) Representative immunofluorescence staining of H3K9me2 (left) and quantification relative to DNA  
13 (right) in indicated genotypes and conditions. Scale bar is 10µm.

14 (G) Density plot showing distance of Zfp281-only (pink), Zic2-only (blue) and Zfp281/Zic2 co-bound  
15 peaks (yellow) to nearest TSS.

1 **(H)** Zfp281 (left), Zic2 (middle) and H3K27ac (right) log<sub>2</sub> ChIP enrichment over matched inputs in ESCs  
2 at Zfp281-only (pink), Zic2-only (blue) and Zfp281/Zic2 co-bound (yellow) peaks.

3 **(I)** Cell state-specific Zic2 ChIP log<sub>2</sub>FC between indicated genotypes and cell states at Zfp281-only  
4 (pink), Zic2-only (blue) and Zfp281/Zic2 co-bound (yellow) peaks.

5

6 **EXTENDED VIEW AND APPENDIX FILES:**

7 **Table EV1:** EpiSC reprogramming screen.

8 **Table EV2:** Zfp281, Ehmt1 and Zic2 genomics.

9 **Table EV3:** Zfp281 protein interactors.

10 **Table EV4:** Oligonucleotide sequences.

11 **Appendix File 1:** R code for PC analyses.